STRUCTURE AND DYNAMICS OF SPIN LABEL SIDE CHAINS IN MEMBRANE PROTEIN USING MOLECULAR DYNAMICS SIMULATIONS

Miss Ngoc-lan Le-nguyen

A Thesis Submitted in Partial Fulfillment of the Requirements

for the Degree of Master of Science in Chemistry

Department of Chemistry

FACULTY OF SCIENCE

Chulalongkorn University

Academic Year 2019

โครงสร้างและพลวัติของโซ่ข้างที่ติดฉลากสปินในเมมเบรนโปรตีนโดยใช้การจำลองพลวัติเชิง
โมเลกุล

น.ส.ง็อก-ลาน เลอเหงียน

วิทยานิพนธ์นี้เป็นส่วนหนึ่งของการศึกษาตามหลักสูตรปริญญาวิทยาศาสตรมหาบัณฑิต
สาขาวิชาเคมี ภาควิชาเคมี
คณะวิทยาศาสตร์ จุฬาลงกรณ์มหาวิทยาลัย
ปีการศึกษา 2562
ลิขสิทธิ์ของจุฬาลงกรณ์มหาวิทยาลัย

Thesis Title	STRUCTURE AND DYNAMICS OF SPIN LABEL SIDE CHAINS IN MEMBRANE PROTEIN USING MOLECULAR DYNAMICS SIMULATIONS
By	Miss Ngoc-lan Le-nguyen
Field of Study	Chemistry
Thesis Advisor	Professor PORNTHEP SOMPORNPISUT, Ph.D.

Accepted by the FACULTY OF SCIENCE, Chulalongkorn University in Partial Fulfillment of the Requirement for the Master of Science

.... Dean of the FACULTY OF SCIENCE

(Professor POLKIT SANGVANICH, Ph.D.)

THESIS COMMITTEE

.... Chairman

(Associate Professor VUDHICHAI PARASUK, Ph.D.)

.... Thesis Advisor

(Professor PORNTHEP SOMPORNPISUT, Ph.D.)

.... Examiner

(Associate Professor Somsak Pianwanit, Ph.D.)

.... External Examiner

(Assistant Professor Chalermpol Kanchanawarin, Ph.D.)

จี๋อก-ลาน เลอเหงียน : โครงสร้างและพลวัติของโซ่ข้างที่ติดฉลากสปินในเมมเบรนโปรตีนโดยใช้การ
จำลองพลวัติเชิงโมเลกุล. (STRUCTURE AND DYNAMICS OF SPIN LABEL SIDE CHAINS IN
MEMBRANE PROTEIN USING MOLECULAR DYNAMICS SIMULATIONS) อ.ที่ปรึกษาหลัก : พร
เทพ สมพรพิสุทธิ์

การติดสปินตำแหน่งเฉพาะ (SDSL) ร่วมกับสเปกโทรสโกปีอิเล็กตรอนพาราแมกเนติกเรโซแนนซ์ (EPR)
เป็นวิธีที่มีประสิทธิภาพในการสำรวจโครงสร้างและการเปลี่ยนแปลงของระบบที่ซับซ้อนทางชีวภาพ สปินไนตรอก
ไซด์เป็นโพรบที่ใช้กันอย่างแพร่หลายมากที่สุดสำหรับ SDSL ในการศึกษาโครงสร้างและหน้าที่ของสารชีวโมเลกุล
อย่างไรก็ตามพฤติกรรมของสปินไนตรอกไซด์ยังไม่เป็นที่เข้าใจกัน การศึกษาครั้งนี้มีวัตถุประสงค์เพื่อศึกษาสมบัติทาง
โครงสร้างและพลวัตของสปินเลเบลในโดเมนรับรู้ศักย์ไฟฟ้า (VSD) ของ KvAP ซึ่งเป็นโพแทสเซียมแชลนัลจาก
แบคทีเรียอาร์เคียที่อาศัยในอุณหภูมิสูง *Aeropyrum pernix* โดยใช้การศึกษาพลวัติเชิงโมเลกุล (MD) ได้ทำการจำลองพล
วัติเชิงโมเลกุลของ KvAP-VSD แบบไม่ติดสปินและแบบติดสปินจำนวนทั้งหมด 132 โครงสร้าง (การติดสปินที่
ตำแหน่งเรสซิดิวซ์ตั้งแต่ 20 ถึง 151) ในฟอสฟอลิพิดไบเลย์ เพื่อประเมินพลวัตของสายโซ่ไนตรอกไซด์สปินเลเบลใน
โปรตีนเมมเบรน ได้สำรวจความยืดหยุ่นของโครงสร้าง, ความอิสระของคอนฟอร์เมชันจากพันธะหมุนได้และการวาง
แนวของสายโซ่ไนตรอกไซด์เพื่อความเชื่อมโยงกับการเคลื่อนไหวภายในของสปินเลเบลในสภาพแวดล้อมทางจุลภาค
ที่แตกต่างกัน การวิเคราะห์ข้อมูล MD แสดงให้เห็นว่าพลวัตของแบคโบนระหว่างโปรตีนที่ไม่ติดสปินและติดสปินมี
ความคล้ายคลึงกัน ความอิสระของคอนฟอร์เมชันจะแปรผันตามสภาพแวดล้อมโดยรอบ การเคลื่อนที่ของสปินเลเบล
นั้นถูกจำกัดภายในเมมเบรนมากกว่าด้านนอกของเมมเบรน จากการจำลอง พันธะหมุนได้ภายในสายโซ่ของไนตรอก
ไซด์ให้ค่าที่แตกต่างกันของมุมไดฮีดรัล ซึ่งบ่งบอกถึงพลวัติที่แตกต่างกันของสปินเลเบลในสภาพแวดล้อมที่แตกต่าง
กัน กราฟฟังก์ชั่นการกระจายเชิงรัศมีระหว่างสปินเลเบลและสภาพแวดล้อมสามารถนำไปสู่จัดชนิดของสปินเลเบล
ได้แก่ ชนิดสัมผัสกับน้ำ ชนิดสัมผัสไขมัน และชนิดฝังอยู่ในโปรตีน พลวัติของสายโซ่สปินเลเบลลดลงตามลำดับ
ต่อไปนี้: ชนิดสัมผัสกับน้ำ > ชนิดสัมผัสไขมัน> ชนิดฝังอยู่ในโปรตีน ผลการจำลองด้วย MD ถูกเปรียบเทียบกับข้อมูล
ผลการทดลองจากเทคนิค EPR การศึกษาช่วยให้ความเข้าใจรายละเอียดเกี่ยวกับโครงสร้าง คอนฟอร์เมชันและพลวัติ
ของสปินเลเบลได้มากยิ่งขึ้น

สาขาวิชา   เคมี   ลายมือชื่อนิสิต ....

ปีการศึกษา   2562   ลายมือชื่อ อ.ที่ปรึกษาหลัก ....

6172120223 : MAJOR CHEMISTRY

KEYWORD: MEMBRANE PROTEIN, VOLTAGE-SENSING DOMAIN, NITROXIDE SPIN LABEL, SPIN LABELING, MD SIMULATIONS

Ngoc-lan Le-nguyen : STRUCTURE AND DYNAMICS OF SPIN LABEL SIDE CHAINS IN MEMBRANE PROTEIN USING MOLECULAR DYNAMICS SIMULATIONS. Advisor: Prof. PORNTHEP SOMPORNPISUT, Ph.D.

Site-directed spin labeling (SDSL) combined with electron paramagnetic resonance (EPR) spectroscopy is a powerful approach to explore the structure and dynamics of biological complex systems. Nitroxide spin label is the most widely used probe for SDSL in the study of structure and function of biomolecules. However, the behavior of the nitroxide spin label is not well understood. This study aims to characterize the structural and dynamical properties of the spin label in the voltage-sensing domain (VSD) of KvAP, a potassium channel from the thermophilic archaea *Aeropyrum pernix* by mean of molecular dynamics (MD) studies. MD simulations for unlabeled and a total of 132 spin labeled KvAP-VSD models (on attachment for the residue position from 20 to 151) were carried out in a phospholipid bilayer to evaluate the dynamics of the nitroxide spin label side chain in membrane proteins. Structural flexibility, conformational freedom of rotatable bonds, and orientation of the nitroxide side chain were investigated in relation to the spin label internal motion in different microenvironments. The analysis of MD data showed that the backbone dynamics between the unlabeled and spin-labeled proteins were similar. The conformational freedoms of the nitroxide side chain vary with the surrounding environments. The spin label motion is more restricted inside the membrane than the outside membrane. From the simulations, the rotatable bonds within the nitroxide side chain adopt distinct values of dihedral angles indicating different dynamics of the spin label in different environments. The radial distribution function plots between the spin label and the nearest-neighbor surroundings allow to categorize the spin labels into water exposure, lipid-exposure, and protein burial. The dynamics of the spin label side-chains decreases in the following order: water-exposed > lipid-exposed > buried type. The MD results were compared with available experimental EPR data. The study provides a detailed understanding of the structure, conformation, and dynamics of the spin label.

Field of Study:	Chemistry	Student's Signature	
Academic Year:	2019	Advisor's Signature	

ACKNOWLEDGEMENTS

TABLE OF CONTENTS

จุฬาลงกรณ์มหาวิทยาลัย

CHULALONGKORN UNIVERSITY

LIST OF TABLES

LIST OF FIGURES

Chapter 1

INTRODUCTION

1.1   Membrane protein

Cell membranes are essentially constituted by membrane lipids and membrane proteins in the presence of a certain amount of carbohydrates as shown in Figure 1.1. Membrane proteins (MPs) are observed much more structurally and functionally diverse than membrane lipids. They have important functional roles involved in ion and molecule conduction, energy transduction, cell integrity, and cell-cell interactions.

Extracellular
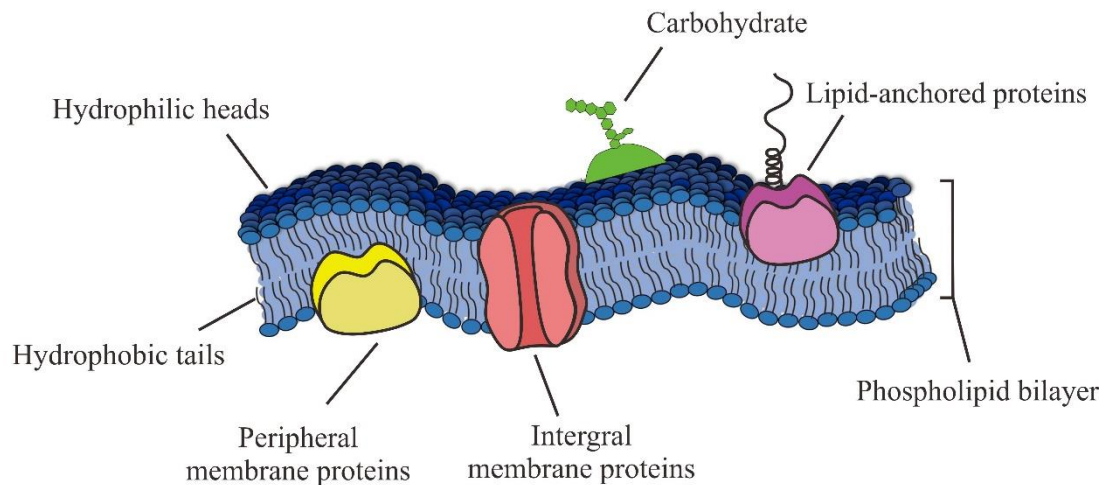
Intracellular

Figure 1.1 Schematic diagram of some typical membrane proteins in a cell membrane

However, MPs are complicated to analyze in their native body cells, due to their embedding in the membrane lipids. In particular, the crystallization process of MPs has been nontrivial and elusive, owing to the difficulties when overexpressing them in bacteria and denaturation when removing from their native environment. Their poor water solubility has hampered the crystallization – an essential stage in X-ray crystallography. That imposes the presence of detergents to render membrane proteins water-soluble. However, there is no universal detergent that works for all membrane proteins. More importantly, they can also alter conformation and function of membrane proteins since they hinder inter- and intra-molecular protein-detergent interactions. Taken together, these aspects lead to the difficulties of experimental techniques in characterizing the MPs structure. Although one third of the coded protein in the human genome

encodes membrane proteins, it has been found around 1-2% of the total available structures in the Protein Data Bank (PDB) systematically elucidated (1). Moreover, roughly over 50% of all FDA approved medicinal drugs target membrane proteins (2,3).
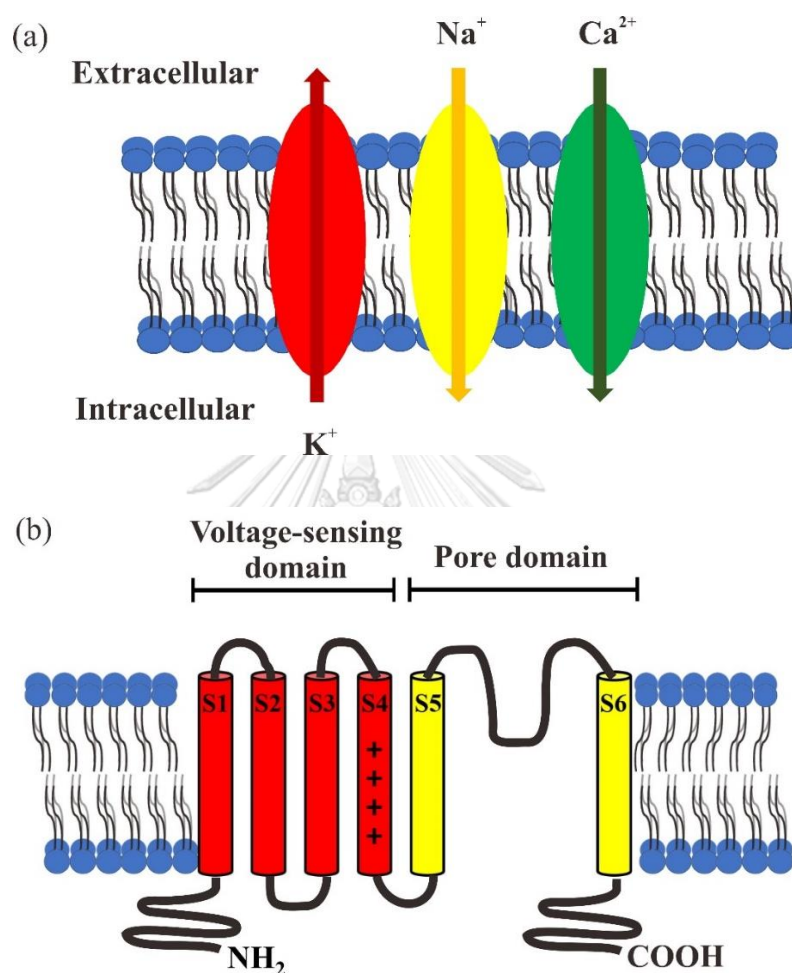
Figure 1.2 Schematic diagram of voltage-gated ion channel (a) specified by individual ions and (b) typical structure with six segments (S1-S6) including voltage-sensing domain (VSD, S1-S4)

Ion channels are the primary target for the drug development. They are responsible for a variety of physiological functions such as neural transmission, cell signaling, regulation and transduction etc. There are different types of ion channels: voltage-gated ion channels, ligand-gated ion channels, mechanically–gated ion channels, and some leak channels. Voltage-gated ion channels are the largest superfamily of ion channels. They comprise primarily of potassium K^+, sodium Na^+, and calcium Ca^{2+} channels as represented in Figure 1.2a. Ion channels of this class share common structural features including a canonical voltage-sensing domain (VSD) and pore

domain (PD) as shown in Figure 1.2b. The VSD plays a crucial role during voltage activation. The PD is important for the selectivity, permeation and gating for ions.

1.2   Site-directed spin labeling EPR technique

A spin label (SL) agent is a probe molecule that is typically used in spectroscopic study as well as biochemical assay. It contains an unpaired electron. The SL agent can selectively bind to molecules containing a specific function group. Spin labels together with electron paramagnetic resonance (EPR) spectroscopy are commonly employed as external molecules for monitoring local dynamics of protein or biological membranes. Site-directed spin labeling (SDSL) combined with EPR has become a powerful technique allowing us to probe structure and dynamics of particular areas within a protein, to validate protein-protein and protein-ligand interactions, and to characterize structural architecture of proteins.

For the attachment of proteins with spin labels, three main approaches have been currently used so far:

- Spin labeling at cysteine position

- Spin labeling by peptide synthesis

- Spin labeling using nonsense suppressor methodology

The first approach is most commonly one that utilizes the reaction of cysteine substitution mutants in the protein. This approach usually requires that the protein contains only cysteine residues at the desired sites. the cysteine can replace amino acid residue at any position along protein sequence without protein functional changes. Spin label side chains are created by a substitution reaction between sulfhydryl group of cysteine side chain and the spin label reagents (4,5). Among different types of spin labels, nitroxides are widely employed. They are very sensitive and provide insights into the polarity, solvent accessibility, and rotational dynamics of specific sites of the protein. The nitroxide spin labels are potential probes for investigating protein dynamics.
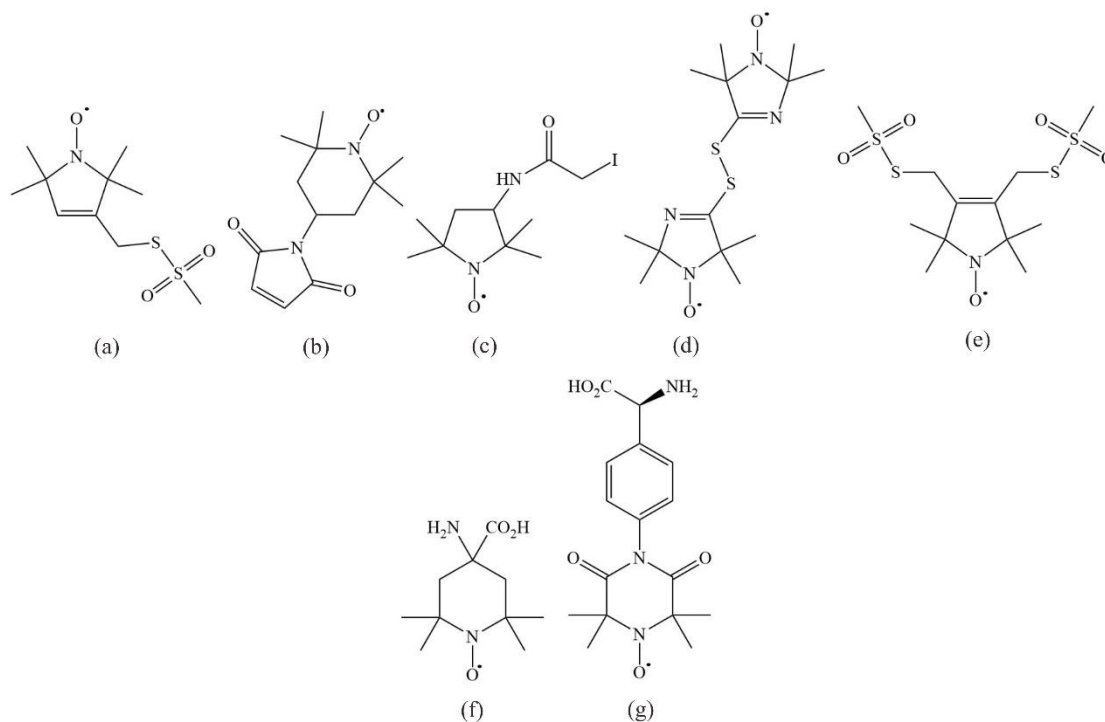
Figure 1.3 Structures of nitroxide spin labels used in the SDSL/EPR study of micromolecules (a) Methanethiosulfonate spin label (MTSSL), (b) maleimide spin label (MSL) N-(1-oxyl-2,2,6,6-tetramethyl-4-piperidinyl) maleimide, (c) iodoacetamide spin label (ISL), (d) bis(1-oxyl-2,2,5,5-tetramethyl-3-imidazolin-4-yl) disulfide (IDSL), (e) bifunctional spin label (BSL), (f) 2,2,6,6-tetramethyl-N-oxyl-4-amino-4-carboxylic acid (TOAC), and (g) 4-(3,3,5,5-tetramethyl-2,6-dioxo-4-oxylpiperazin-1-yl)-l-phenylglycine (TOPP) (6)

There are several nitroxide spin label probes for SDSL combined with EPR spectroscopic studies of biomolecules (7-14) as shown in Figure 1.3 (6). The spin labels in Figures 1.3(a)–1.3(e) are attached to proteins via site-directed mutagenesis while those in Figures 1.3(f)-1.3(g) are incorporated through peptide synthesis. A resulting side chain established by the reactivity of the most flexible commonly applied spin label, (1-oxyl-2,2,5,5-tetramethylpyrroline-3-methyl) methanethiosulfonate spin label (MTSSL), with the cysteine residue of the protein is introduced in Figure 1.4, commonly abbreviated by R1 side chain.

In this study, the structure and dynamics of spin label side chains at all amino acid positions of the X-ray structure of the voltage-sensing domain (VSD) of a potassium channel from the archeabacterium *Aeropyrum Pernix* (KvAP) (15) were investigated using all-atom molecular

dynamics (MD) simulations. The dynamical properties are compared to the experimentally-determined mobilities obtained from the previously published EPR data (16).
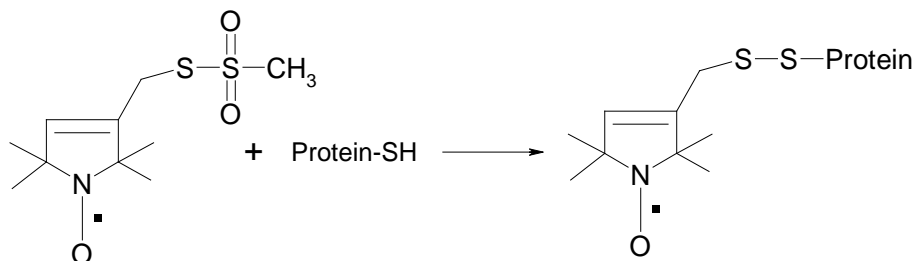
Figure 1.4 Spin label side-chain (R1) produced by reaction between a cysteine residue and MTSSL

1.3 Literature review

1.3.1 Site-directed spin labeling EPR technique for studying membrane proteins

The motion of spin label side-chain is highly dependent on its neighboring side chains and secondary structure constituents in its exposed environment. Therefore, the local structural and dynamical properties of the protein can be reported. A pioneering work of Hubbell and co-workers introduced SDSL EPR technique around 30 years ago (17). Remarkably, one of the first studied proteins was a membrane protein. Since then it has become a commonly complementary tool in structural biology. In the spin labeling procedure, one can intentionally select the location of interest, or scan along the protein sequence seeking for differences along the protein chain. In addition, the relationship between the dynamics of the spin label side-chain and protein structure has been extensively studied for T4 lysozyme (18-22)

Using nitroxide-based site-directed spin labeling (SDSL) EPR, membrane protein topology can be investigated (23,24). Functional domains in membrane proteins can be identified applying this method (18). Moreover, there are some essential MPs have been studied in terms of the structure and dynamic properties such as KCNE1, KcsA, amyloid precursor C99 domain, lactose permease, integrin, bacteriorhodopsin, and KvAP-VSD (16,23,25-30). In the study of KvAP-VSD (16), the structural transition between the "down" and "up" conformations was investigated using SDSL EPR spectroscopic approaches. Spin labels were attached at residues 16–147 on the VSD one at a time in both PCPG and DOTAP liposomes. Then, mobility and solvent accessibility at each site of KvAP-VSD in the liposomes were calculated, applying EPR spectroscopy studies.

The SDSL/EPR approach has been applied to study the structure and dynamics of KCNE1 which plays a vital role in modulating the function of the voltage‑gated potassium ion channel (K_v) (25,31). The EPR data indicated that the motion of nitroxide spin label side chains attached in the KCNE1 transmembrane domain (TMD) are more restricted than those located in the extracellular area of KCNE1. A study on the amyloid Obr2A is another recent instance of employing nitroxide spin labeling combined with EPR spectroscopy (32). They varied the concentration of lipids to elucidate the spin label side-chain flexibility.

McCaffrey *et al.* employed a bifunctional spin label in combination with EPR spectroscopy at X-band on phospholamban (PLB) which is an integral membrane protein to find the protein structure (33). The results suggested that EPR data of the spin label can be utilized to clarify the direction and dynamics of an integral membrane protein segment in magnetically aligned bicelles. Using that technique and TOAC spin labeling at multiple sites, the correct helical tilt angle and dynamical feature of the AchR M2δ peptide was recently determined by the Lorigan group (34).

Besides, SDSL/EPR can be used to estimate distances from within or between the spin labeled sites in MPs. This distance information can be calculated from two spin labels either in the same protein or different proteins (35) based on the magnetic dipolar interactions between their unpaired electrons. These distances can be measured to monitor the secondary, tertiary, and quaternary structure of MPs (36).

1.3.2 Computational studies of the nitroxide side chain in membrane protein

The main impact on continuous wave EPR spectra and on nuclear spin relaxation times initiates from fluctuations of dihedral angles χ_1 to χ_5 as introduced in Figure 1.5. For the nitroxide spin label MTSSL, the appropriate angles χ_1 to χ_5 are shown in Figure 1.6 (37). Depending on these rotational conformers, the distance from C_α to the unpaired electron which localized to the N‑O bond of nitroxide is around 7 Å (38).

In the case of R1 side chain, quantum mechanical ab initio methods provided precise energetics for a variety of conformational states of R1 (39-41). However, in general, these approaches are computationally too demanding for proteins in large scales. More importantly, they fail to observe thermal fluctuations. Based on classical force fields molecular dynamics (MD) simulations offered a more realistic substitute method to investigate the conformational dynamics

of the R1 side chains (42,43). The results acquired from the MD simulations analysis agreed with the available X-ray crystallography data (44).
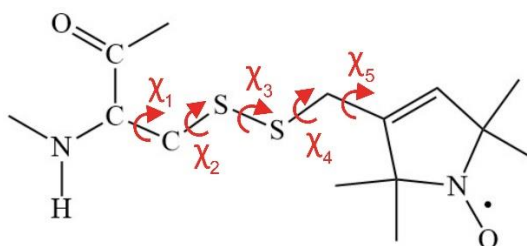
Figure 1.5 Structure of residue R1 formed by reaction of the MTSSL with a cysteine residue with dihedral angles χ_1–χ_5 noted in red

In 2010, Gunnar Jeschke group (45) showed that libraries of around 200 rotamers from a repetitive projection of a long molecular dynamics trajectory of the unrestrained MTSSL onto a canonical dihedral angles ensemble as shown in Figure 1.6 (black lines). It provided a representation of the fundamental trajectory sufficient for EPR distance measurements. To characterize the set of spin label rotamers on a single protein position, analysis of rotamers was carried out on spin labeled T4 lysozyme mutants. An MD simulation study of MTSSL attached to a polyalanine α-helix at its central site in an explicit solvent was performed (43). They simulated EPR spectra using the MD trajectories and comprising global dihedral angles diffusion appropriate for T4 lysozyme tumbling in solution as presented in Figure 1.6 (red bars).

Using Density Functional Theory (DFT) computations, Wayne L. Hubbell *et al.* performed conformational analysis of the R1 side chain in an α-helix to calculate the energies of rotameric states in solution (39). The energy minima corresponding to the χ_1–χ_3 rotamers were shown in Figure 1.6 (green bars). Besides, the blue lines in Figure 1.6 represented the dihedral angles observed in protein crystal structures attached MTSSL. These data were collected from different references (22,46-56) by Gunnar Jeschke (37). For angles χ_1, χ_2, and χ_4, potential energy minima were found at -60°, 60°, and 180°. Meanwhile, χ_3 and χ_5 potentials have minima at -90° and 90°. The dihedral angles distributions obtained from MD simulations of MTSSL attached into the central cysteine of a pentadeca glycine helix approximately consistent with the minima of expectation (57).

In MD simulations, transitions between different positions of χ_1 and χ_2 are slower (58) than those of χ_4 and χ_5. Besides, the dynamics of the MTSSL probes to α-helix was studied to

rationalize its impacts on EPR spectra (41). Conformational profiles of the side chain bonds were calculated by ab initio method. A limited number of allowed rotamers was determined that undergo rotational oscillations and jumps. In particular, the transitions frequency between χ_5 states are affected by the other rotamers, especially on χ_4, and can be very high for some conformations due to an almost flat χ_5 potential.
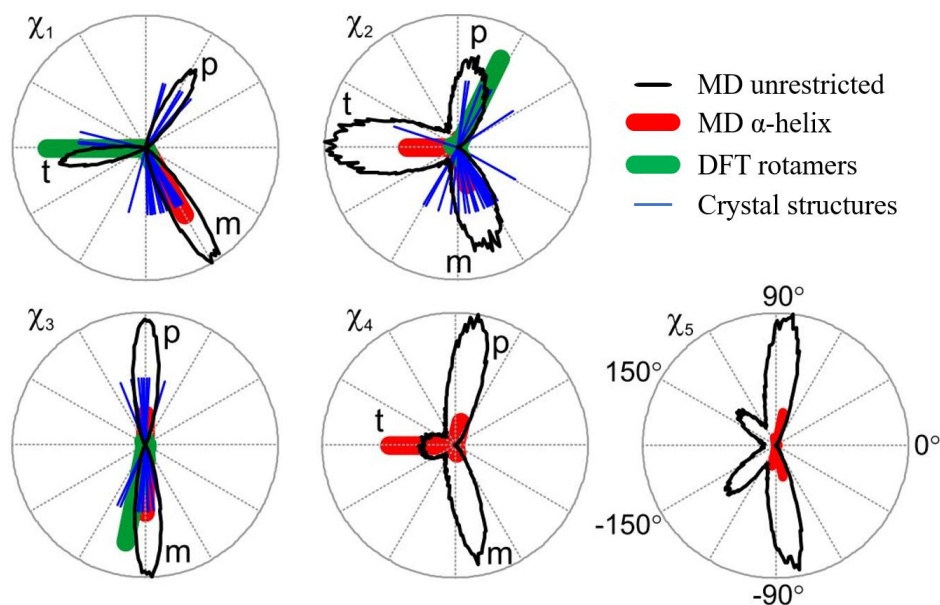
Figure 1.6 Distribution of dihedral angles in the spin-labeled residue R1 formed by reaction of the MTSSL with a cysteine residue (37); p, t, and m states stand for plus, trans, and minus values of angle, respectively, which are alternative for gauche(+), trans, and gauche(-) nomenclature by IUPAC.

1.4 Objectives

1. To model structures of cysteine-mutated membrane protein with nitroxide spin label attaching at various positions

2. To investigate structural and dynamic properties of spin label in membrane protein

3. To categorize all spin label sites in the protein based on different local environments

Chapter 2

METHODOLOGY

2.1 Constructing structure models of the spin labeled protein

The crystal structure of KvAP-VSD (PDB code: 1ORS) was used to construct protein structure models containing the nitroxide spin label side chain. In the study, the spin label was attached to an amino acid position one at a time throughout the KvAP-VSD structure. The structure coordinates available in PDB consist of four transmembrane segments (TMs) spanning from residues 20 to 151 (132 residues). Therefore, we constructed a total of 132 structure models attached with the spin label moiety through the CHARMM-GUI web server (59) (http://www.charmm-gui.org), (15) as illustrated in Figure 2.2(a, b). All the 132 structure models were subsequently subjected to build the protein-lipid systems for membrane protein simulations which were described in the next section.

2.2 Molecular dynamics details

2.2.1 Preparation of simulation systems

In the next step, each spin label-attached KvAP-VSD was embedded in the phospholipid bilayer of POPC (1-palmitoyl-2-oleoyl-sn-glycero-3-phosphocholine). The structure of POPC molecule is shown in Figure 2.1. The protein-lipid systems were solvated with the TIP3P water molecules (60). The simulation box was roughly $84 \times 81 \times 90$ Å^3 in size. The Na$^+$ and Cl$^-$ counterions were used to neutralize the systems with the salt concentration of 0.1 M. Figure 2.2 shows one example of preparing the system by CHARMM-GUI in Figure 2.2(a, b) and VMD software in Figure 2.2(b, c).
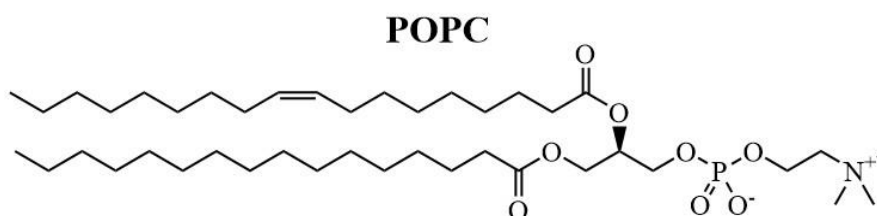
Figure 2.1 Chemical structure of POPC molecule

(a)   (b)   (c)
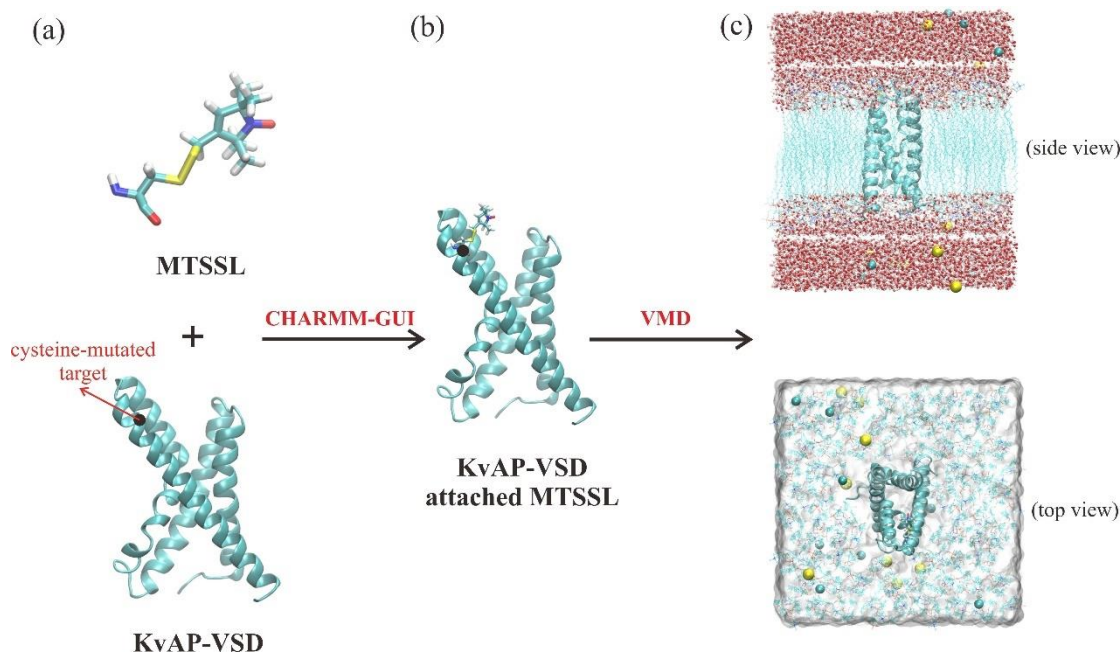
Figure 2.2 An example for constructing systems using CHARMM-GUI and VMD software

2.2.2 MD simulations

An all-atom molecular dynamics (MD) simulation was performed using NAMD program (version 2.11) (61). Periodic boundary conditions were applied. The CHARMM36 (62) force fields were used to calculate the interatomic interactions for protein and lipid. The force field parameters of the spin label were also provided from CHARMM-GUI platform. The long-range electrostatic interactions are calculated by the particle mesh Ewald (PME) method (63). The simulation time was 100 ns for testing of some random systems and then 10 ns for all, which was discussed in more detail in the part of system stability. During the simulation time, the average temperature and pressure were controlled at 298 K and 1 atm using Langevin dynamics and Nosé-Hoover Langevin piston method, respectively. The switch and cutoff were 10 and 12 Å, respectively. The SHAKE algorithm (64) was employed. The time step was 1 fs. MD trajectories were saved every 1 ps.

2.3 Molecular dynamics trajectory analysis

To study the conformation dynamics of spin label side chains in the membrane protein, we did calculate the root-mean-square deviation and root-mean-square fluctuation quantities. In addition, we applied the radial distribution function (RDF) method to categorize the spin label side chains in different local environments (water, lipid, and buried site).

2.3.1 Root-mean-square deviation calculations

Root-mean-square deviation (RMSD) was calculated as a quantitative measure of the similarity between two superpositions of atoms. Therefore, it can be used to evaluate how the system deviates from the initial crystal conformation. The RMSD value of the backbone Cα atoms is measured in Å, using the following equation:

$$RMSD\left(t_1, t_0\right) = \left[\frac{1}{M} \sum m_i \| r_i\left(t_1\right) - r_i\left(t_0\right) \|^2 \right]^{\frac{1}{2}} \quad (1)$$

where M is the mass of all atoms, m_i and r_i are the mass and position of atom i, respectively; and time t_0 refers to the reference position (crystal structure).

2.3.2 Root-mean-square fluctuation calculations

To determine the structural variation, the residue-by-residue root-mean-square fluctuation (RMSF) of the backbone Cα atoms or nitrogen atom of nitroxides (for spin label side chains) from their average locations were computed by the formula as follows:

$$RMSF_i = \left[\frac{1}{T} \frac{1}{M} \sum m_i \langle \left(r_{ij}\left(t\right) - \bar{r}_{ij}\right)^2 \rangle_{MD} \right]^{\frac{1}{2}} \quad (2)$$

where T is the equilibrated MD trajectories.

The dynamics of spin label side chains measured from RMSF were compared to the experimental data (16).

2.3.3 Radial distribution function

The radial distribution function $g(r)$ was computed to reveal the average distribution of the atoms in the surrounding of spin label side chains. It can be represented by a pair correlation functions $g_{AB}(r)$ between two atoms A and B as shown in equation (3). These quantities can be used to characterize the side chain sites based on the different immediate environments such as water, lipid, and membrane protein itself.

$$g_{AB}\left(r\right) = \frac{\langle \rho_B\left(r\right) \rangle}{\langle \rho_B \rangle_{local}} \quad (3)$$

where ρ_B is the probability density of finding atom B as a function of distance (r) between A and B atoms.

All the method described above are summarized in Figure 2.3
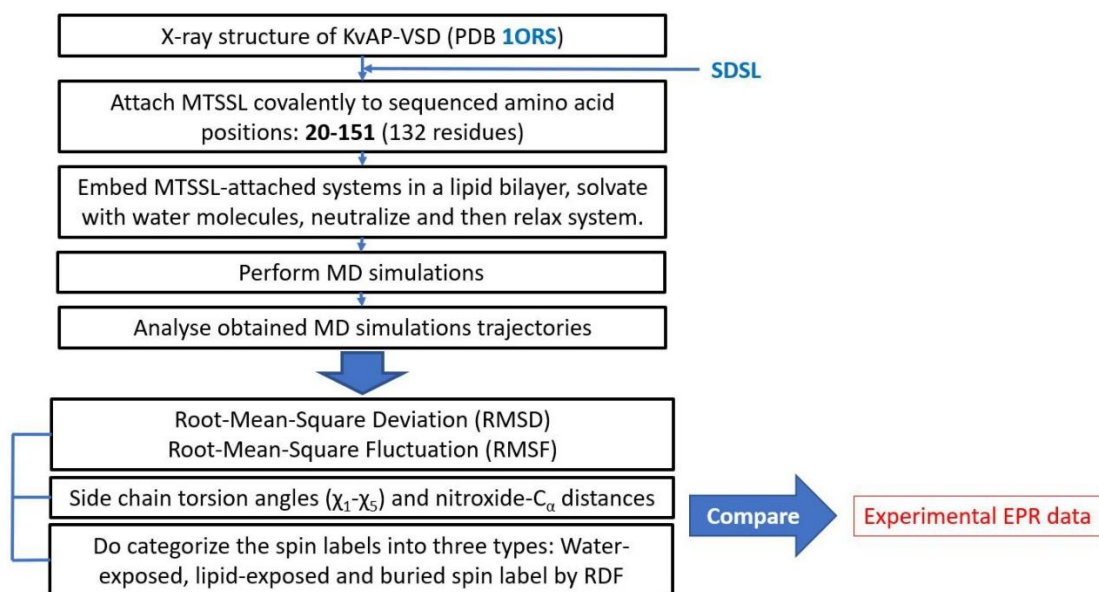
Figure 2.3 Diagram of the main steps in this study
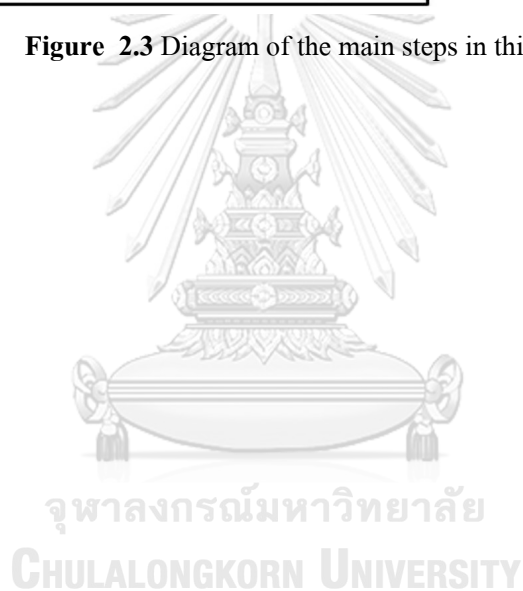
Chapter 3
RESULTS AND DISCUSSION

As staged, this study aims to characterize the geometrical and dynamical properties of the spin label in membrane protein systems. We have performed MD simulations of KvAP-VSD as it represents a simple model system to study the structure and mobility of nitroxide spin labels. The voltage sensor domain of KvAP consists of 132 amino acid residues (the residues numbered from 20 to 151) with four transmembrane segments (S1-S4) as described in Figure 3.1. The KvAP structure has been resolved at 1.9Å resolution. In addition, the EPR data of spin labeled KvAP-VSD are available for a detailed interpretation of the position dependent behavior of the spin label in different surrounding environments such as in the membrane-exposed regions, water-exposed regions and buried regions.
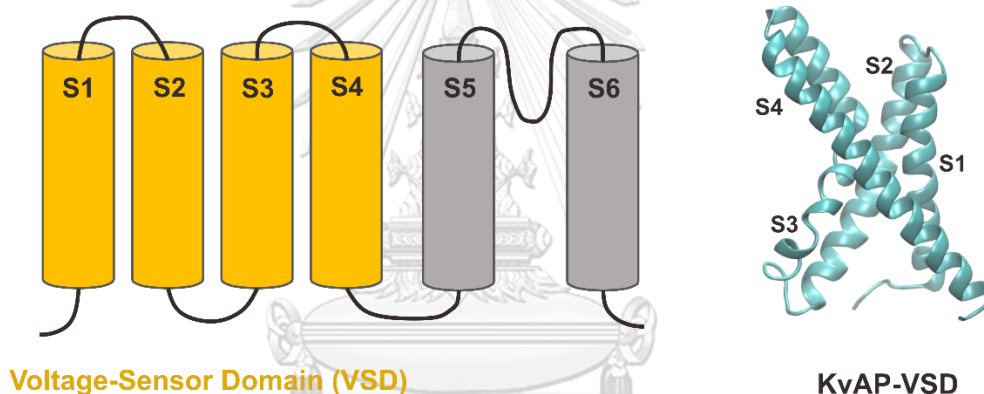
Figure 3.1 Schematic diagram of voltage-sensor domain (VSD) with four segments (S1-S4) in typical structure of voltage-gated ion channels (S1-S6) and structure of KvAP voltage-sensor domain (KvAP-VSD)

3.1   Characterization of the backbone dynamics

It should be noted that there were a large number of the spin labeled KvAP-VSD systems to be carried for MD simulations (a total of 132 independent runs). It is necessary to reduce the CPU time to compensate computational costs. We decided to perform the simulation of 10-ns in length as we were interested only local motion of the spin label side chain. Moreover, the experimental EPR data indicated that the protein structure was minimally perturbed by the presence of nitroxide side chain. However, it is important to examine a range of spin label conformations which were sufficiently captured by MD simulations with fairly small time and length scales. As a control, four systems were randomly chosen for carrying out a relatively long simulation (100-ns).

These are the unlabeled and three spin-labeled KvAP-VSD systems which are denoted as KvAP-VSD, SL35, SL71, and SL89, respectively. The numbers, 35, 71, and 89 correspond to the residue number where the spin label has been attached. Structure comparison between those from MD snapshots and the reference x-ray was analyzed using root-mean-square deviation (RMSD) calculation. The RMSD values were computed based on the backbone atoms of the protein. The MD snapshot structures were superimposed on to the reference X-ray structure (15) to discard translation and rotation of the protein molecule. The RMSD plots as a function of simulation time of the four selected systems were illustrated in Figure 3.2.
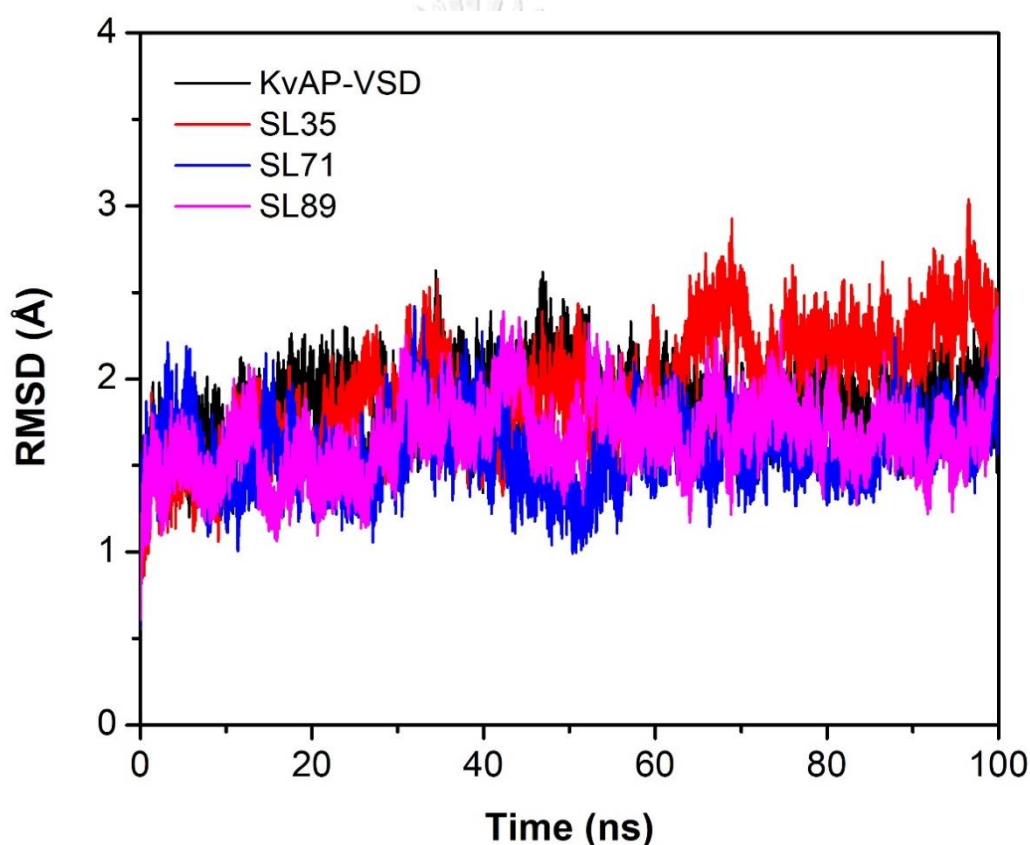
Figure 3.2 Backbone RMSD profiles of 100 ns MD trajectories of KvAP-VSD, SL35, SL71, and SL89

As can be seen in Figure 3.2, the backbone RMSDs in all the equilibrated production trajectories kept stable within 1.5-2.5 Å. It has also shown that in most cases it required less than 10ns for the backbone atoms to reach equilibrium. After equilibration has been reached, backbone conformations fluctuate very little with respect to their own average. To illustrate no significant

different in the global structures during the early time and near final time of the simulation, we compared the C_α atom-RMSDs of SL35, SL71 and SL89 average over the first 10 ns and last 10 ns (the 90-100 ns interval). As summarized in Table 3.1, there were no essential difference in the movement of the backbone during the first 10 ns and last 10 ns, with the deviation of C_α-RMSDs from 0.16-0.38 Å.

Table 3.1 Average C_α atom-RMSD for the first 10ns and the last 10ns of 100 ns MD simulations

System	Average RMSD (Å)		Deviation (Å)
	The first 10 ns	The last 10 ns	
SL35	1.16	1.00	0.16
SL71	0.62	0.92	0.30
SL89	0.91	1.29	0.38

The distribution probability of C_α-RMSD can provide structure and dynamics information of the protein. For SL35, SL71, and SL89, there were slightly shifted in the C_α-RMSD distribution from the first 10ns to last 10ns of simulations (Figure 3.3). This suggested that the VSD structure remains unchanged relative to their average structure during the simulations. Furthermore, global dynamics at the early and final simulation times were nearly unaltered as shown by a similar distribution shape during the first and last 10ns of simulations. From the results, we can conclude that the VSD has reached a well-defined structural equilibrium after few nanoseconds of simulations. It also implied that MD simulation of ten nanosecond timescale for KvAP-VSD would be sufficient to capture the spin label dynamics with an amplitude of the nitroxide motion in a range of 1-5 Å. This finding has led us to set the simulation time length to 10ns for the remaining 129 systems since we were interested to investigate the conformational dynamics of nitroxide spin label side chains.
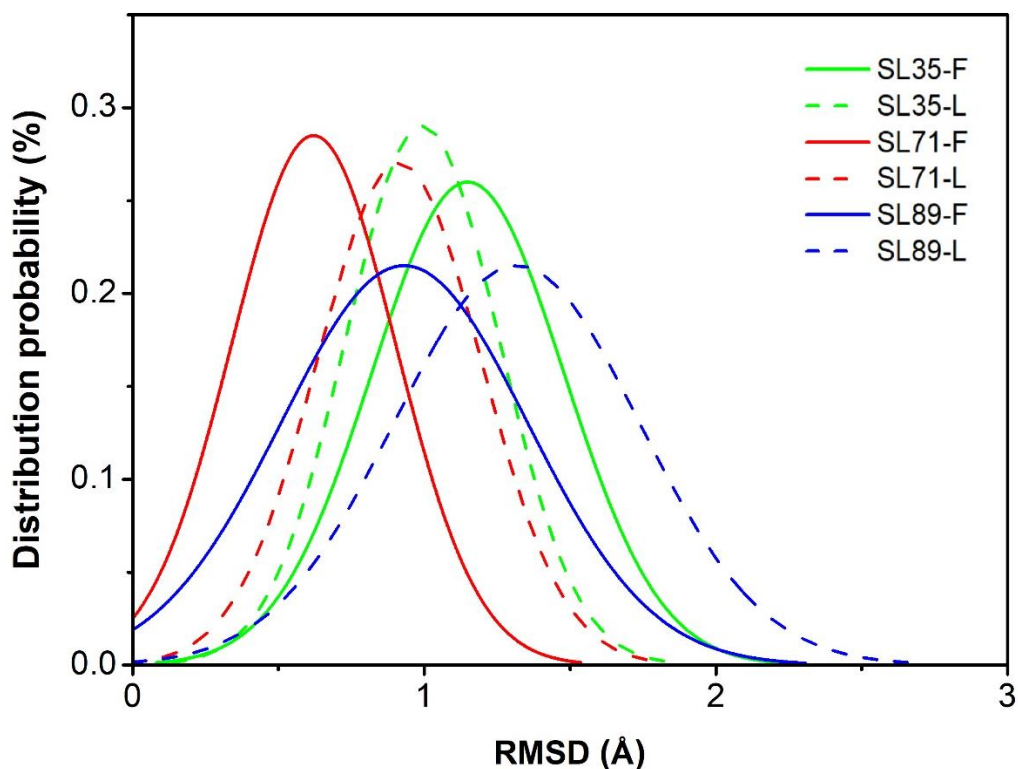
Figure 3.3 Distribution probability of Cα-RMSD of SL35 (green), SL71 (red), and SL89 (blue) over the first 10 ns (SL35-F, SL71-F, SL89-F; solid lines) and the last 10 ns (90-100 ns interval) (SL35-L, SL71-L, SL89-L; dash lines).

3.2 Dynamics properties of spin label side chains

To identify the mobility of spin label relative to the protein motion, the root-mean-square fluctuation (RMSF) with respect to the average structure was analyzed using the simulation time duration of 5-10 ns. Figure 3.4 shows backbone RMSF values for 132 positions of spin labeled KvAP-VSD in comparison with those of unlabeled VSD. As can be seen, a relatively high RMSF at the N- and C- terminals, the loops (S12, S23, and S34) between transmembrane segments usually possessed the prominent peaks of RMSFs, revealing their greater structure flexibilities than the S1, S2, S3, and S4 segments. The mobility of transmembrane segments was reduced in comparison with that of the non-transmembrane regions. The movement of the backbone inside membrane is more restricted in part due to the formation of stable α-helix whereas the greater motion of the backbone outside membrane is attributed by flexible random-coil. From the results, the protein is less flexible**.**
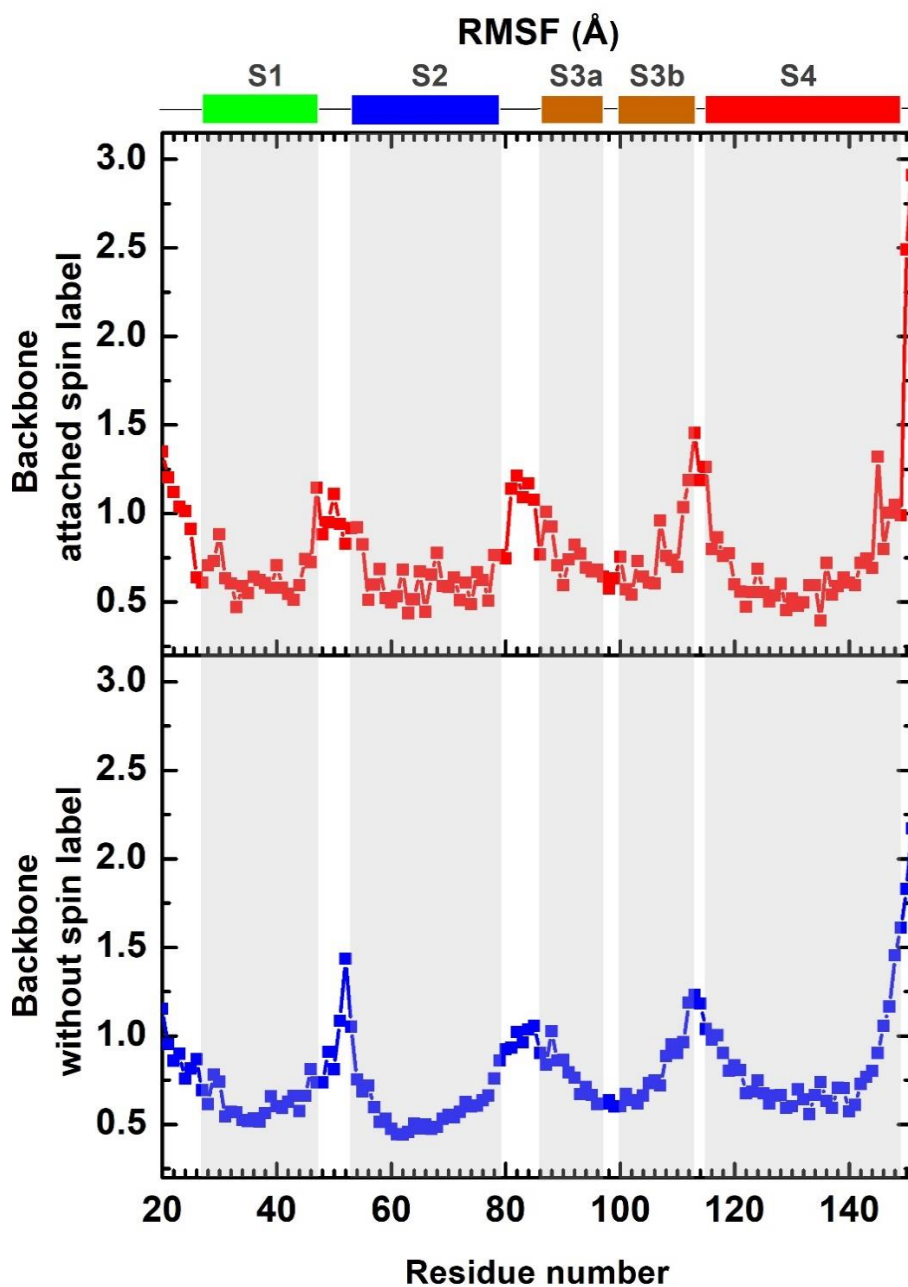
Figure 3.4 RMSF of backbone without spin label (blue line) and backbone attached spin label (red line) with the similar pattern. Residues in transmembrane regions (S1, S2, S3 and S4) are highlighted in gray. The S3 helix breaks into S3a and S3b.

In addition, an RMSF comparison between spin labeled and unlabeled KvAP-VSD provides information about the influence of spin label on the protein structure. It was, however, found that the profile pattern of the backbone RMSF of spin labeled KvAP-VSD was not significantly different from that of unlabeled KvAP-VSD. This suggested that attaching the spin

label into the protein did not severely affect KvAP-VSD structure. The MD results were consistent with experimentally-determined EPR data. This also suggested that we can investigate the dynamics behavior of the spin label from our simulation data.
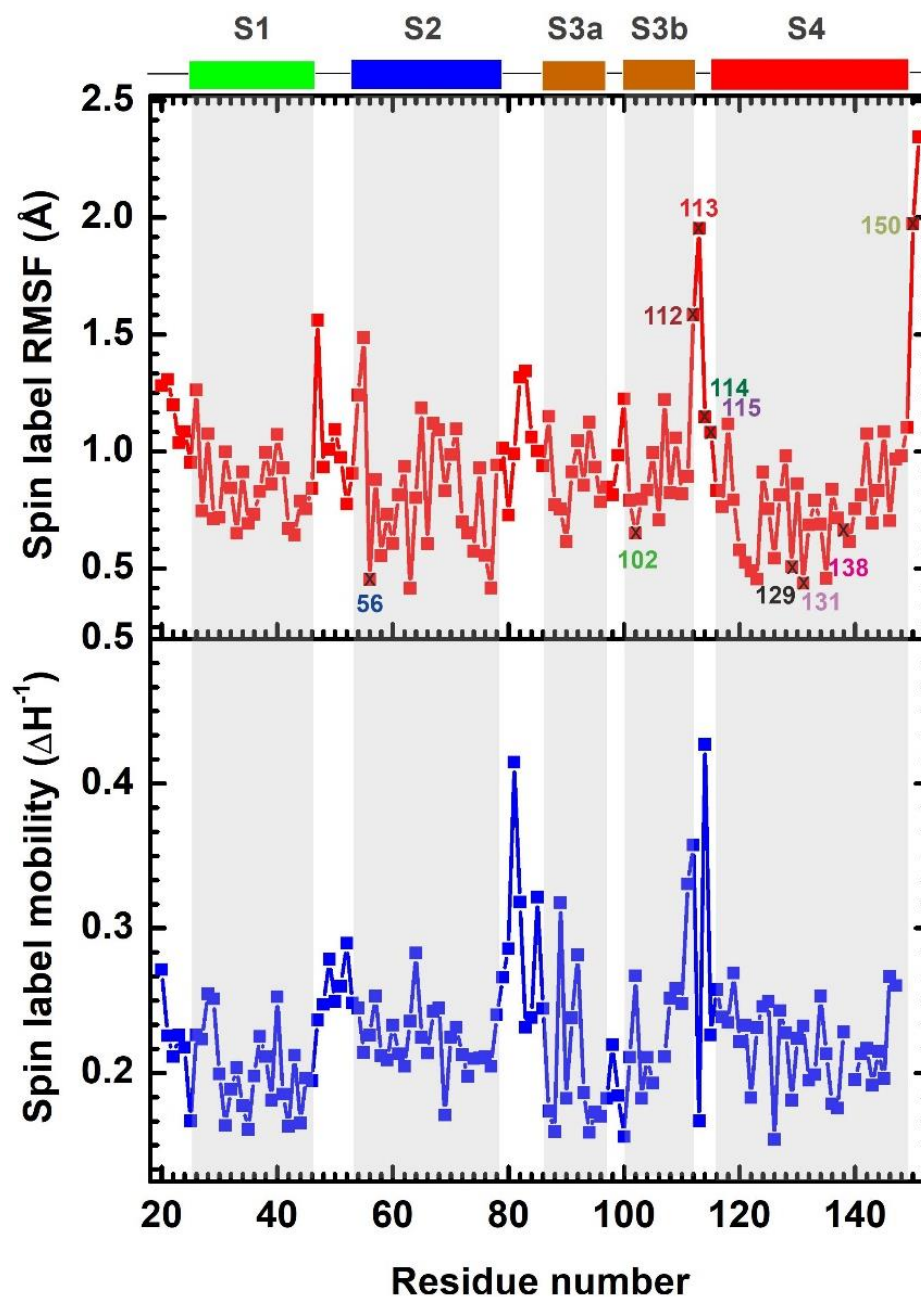
Figure 3.5 RMSF (red line) and mobility (16) (blue line) of spin label side chains. Dynamics of spin label side chains in S3 helix were remarkably varied due to the mid-helix break of S3. Both RMSF and mobility in the plot show the helical periodicity in membrane regions.

The flexibility of each nitroxide side chain on KvAP-VSD was evaluated in terms of RMSF. Figure 3.5 showed a comparison between RMSF of nitroxide side chain and the experimental mobility (ΔH^{-1}). The RMSF profile of transmembrane segments has, on average, a periodic characteristic of helix, similar to the experimental mobility Both RMSF and mobility showed a similar trend in such a way that the spin label mobility was high in the loops and more restricted in membrane regions. This suggested that the dynamics motion of spin label side chains from MD simulations was overall good agreement with the experimental mobility (16). It appears that the spin label with high mobility showed a broader Cα-RMSD distributions (residues 112-115, and 150) whereas that with low mobility (residues 56, 102, 129, 131, and 138) exhibited a sharp Cα-RMSD distributions (Figure 3.6). This suggested that conformational dynamics of the nitroxide spin label was connected with the movement of the protein backbone.
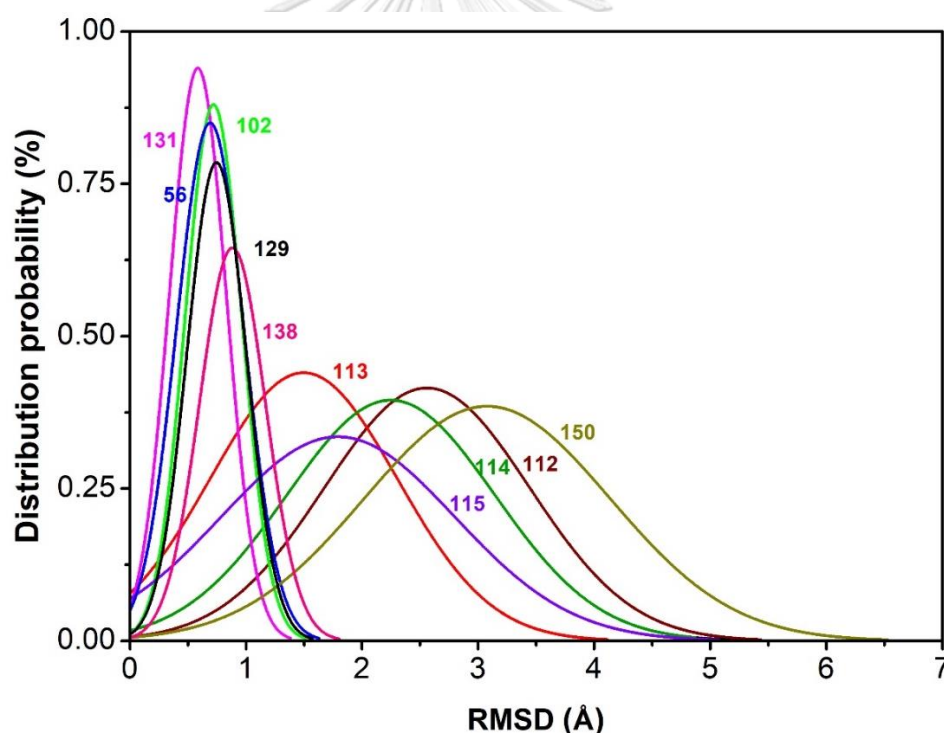
Figure 3.6 Distribution probability of Cα-RMSD of some selected residues 56, 102, 112, 113, 114, 115, 129, 131, 138, and 150. Sharps distributions appear at residues 56, 102, 129, 131, and 138. Broader distributions appear at residues 112-115, and 150.

To visualize the variation of the spin label dynamics with respect to their position on the KvAP-VSD structure, color mapping method was applied for both RMSF (residues 20-151) and mobility (residues 20-147) profiles as illustrated in Figure 3.7. The color ranged from blue to red

to represent from low to high dynamics of the spin label side chains using VMD software. Most areas of blue color located in the intramembrane while the white and red colors commonly appeared near or in extramembrane regions.
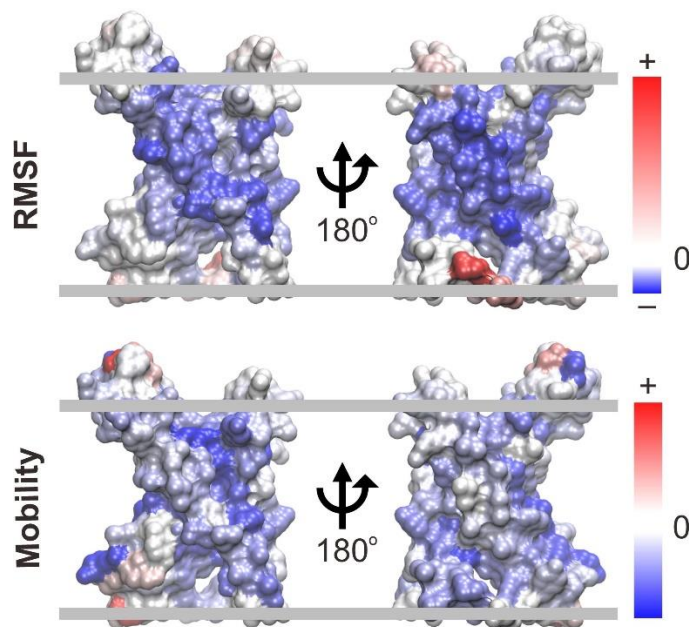
Figure 3.7 Color mapping of the RMSF and mobility data of spin label side chains. Color ranges from blue to red corresponding to the increasing of spin label dynamics using VMD software.

The RMSF and mobility distributions of all spin label side chains in four segments (S1-S4) and loops (S12 and S23) were also calculated and plotted using box charts in Figure 3.8 and Figure 3.9, respectively. There was only one residue connecting S3 and S4, hence S34 loop can be neglected. The average RMSF and mobility from EPR data of R1 side chains in each segment and loops were also computed and shown in Table 3.2.

Table 3.2 Average RMSFs and mobility of spin label side chains in each segment and loop

Average value	S1	S12	S2	S23	S3	S4
RMSF (Å)	0.88	0.96	0.83	1.07	0.98	0.77
Mobility (g^{-1})	0.20	0.26	0.23	0.30	0.22	0.22

The loop S23 shows the largest average of both RMSF (1.07 Å) and mobility (0.30 g^{-1}). The average RMSF of S12 had approximate value with S3, 0.96 ~ 0.98 Å. However, in term of mobility, S12 had higher mobility than S3, 0.26 > 0.22 g^{-1}. For S1, S2, and S4, their average RMSF

and mobility values were all smaller than those of S12 and S23 as seen in Figure 3.8 and 3.9. From the results, spin label side chains in the loops were more mobile than those in the segments.
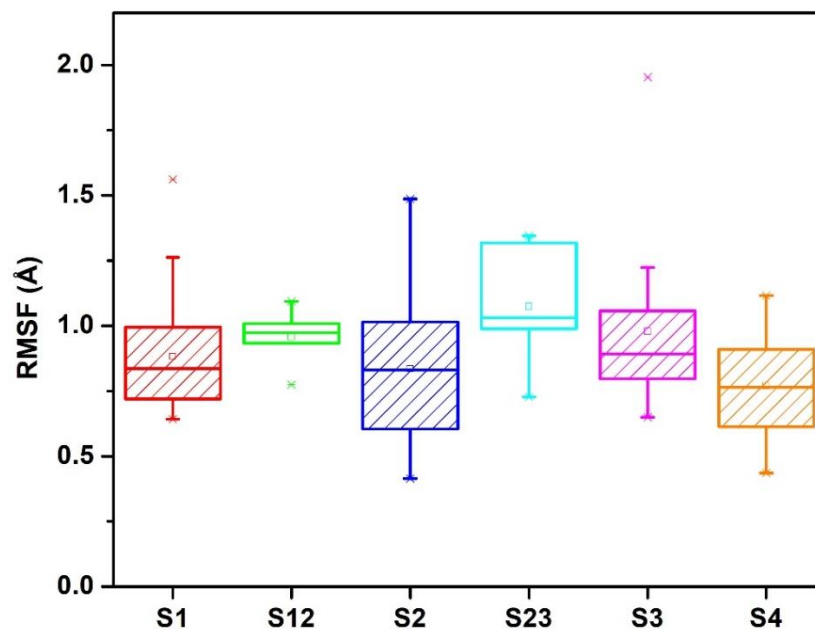
Figure 3.8 RMSF distributions of spin labels in the segments (S1-S4) and the loops (S12 and S23) sites
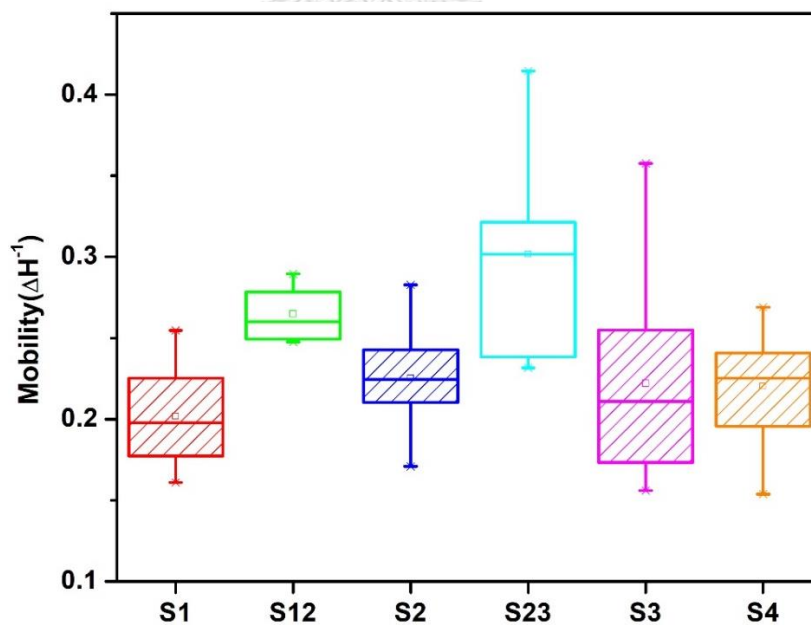
Figure 3.9 Mobility distributions of spin labels in the segments (S1-S4) and the loops (S12 and S23) sites

3.3   Structural fluctuations of spin label side chains

To understand the conformational dynamics of the nitroxide spin label in the membrane system environment, dihedral angles associated with all rotational bonds within the spin label side chain were defined as follows: χ_1: CA-CB, χ_2: CB-SG, χ_3: SG-S2L, χ_4: S1L-C1L, and χ_5: C1L-C1R (Figure 3.10). The rotational motion of the nitroxide spin label linked to these dihedral angles were calculated during the last 1 ns MD trajectories. The dihedral angles averaged over 132 MD systems showed a general tendency of the preferred orientation of the spin label in KvAP-VSD.

The dihedral angles ranged from -180° to +180 whereas the confidence interval was ±30°, using the right-handed rotation rule in which if it represents a clockwise direction with the axis oriented towards the end of the side chain, this angle is positive and vice versa. The central bond of NA-CA-CB-SG (χ_1) rotations were distributed at ±60° and ±180°. For CA-CB-SG-S1L fragment, χ_2 angle values were located at ±75°, ±180°, and slightly changed to ±60°, ±150°, respectively. The CB-SG-S1L-C1L dihedral angles (χ_3) were found at only two regions of 90° and -90° owing to the intrinsic barrier of the disulfide bond (65). The χ_4 dihedral angles in SG-S1L-C1L-C1R configurations were relatively unhindered and the most fluctuated ones (19). In particular, χ_4 ranged from ±60° to ±180°. In the case of χ_5 rotational conformations, they spread from 0-±120° which were restrained by the interaction potential of the S1L atom with the α-CH_3 groups and the 4-H of the nitroxide ring (19).
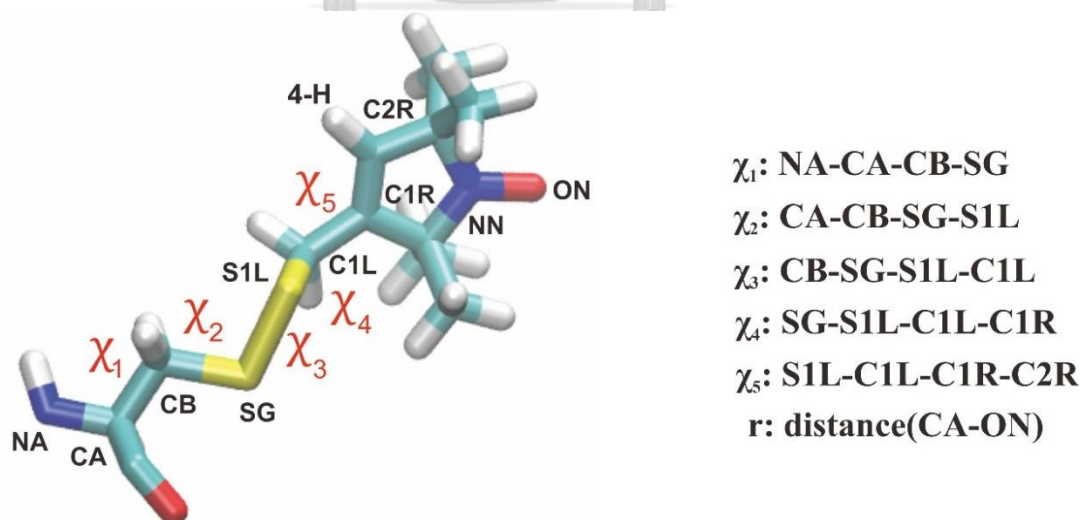
Figure 3.10 Definition of dihedral angles (χ_1- χ_5) of MTSSL and nitroxide-Cα distance (r)

As summarized in Table 3.3 and Figure 3.11, the nitroxide side chain adopts particular conformations implying preferred rotamers of the spin label. All detailed plots of these rotamers were presented in Supplementary figures (Appendices) Figure S1-S15. The values of the χ_1- χ_5 obtained in this study were in good agreement with those obtained by *ab initio* calculations (41) for the spin label attaching in Poly-Ala α-helix (Figure 3.11).

Table 3.3 Average values of the dihedral angles

Type	MD simulations (±30 deg)	*Ab initio* computation (41)
χ_1 (deg)	±60, ±180	-60, +65, ±180
χ_2 (deg)	±60, ±75, ±150, ±180	±75, ±180
χ_3 (deg)	±90	± 90
χ_4 (deg)	±60, ±75, ±90, ±150, ±180	±75, ±180
χ_5 (deg)	0, ±45, ±90	± 8, ± 77, ± 100
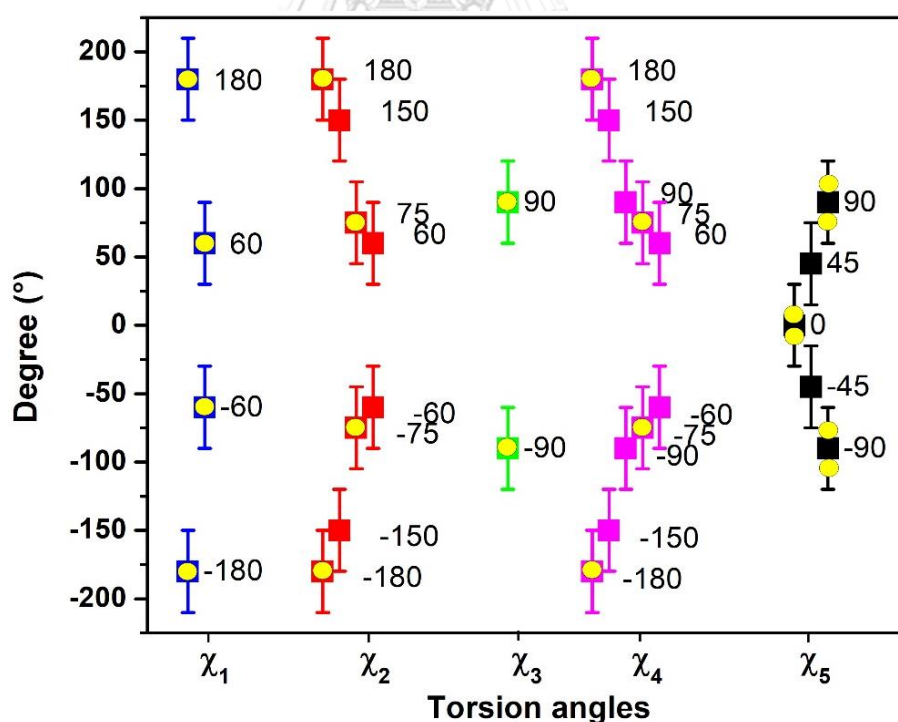
Figure 3.11 Dihedral angle distribution for χ_1, χ_2, χ_3, χ_4, and χ_5 represented by blue, red, green, purple, and black color symbols, respectively. Its average coincides with the value obtained from *ab initio* calculations (yellow circles).

Depending on those rotational conformers, nitroxide-Cα distances were also varied. The average distances of nitroxide-Cα of all spin label side chains in the KvAP-VSD structure were also examined and reported in Figure 3.12. The distance variation was from ~6.5-10 Å and the global average distance is about 8.5 Å as shown by the gray dash line in Figure 3.12. According to De Sensi, S. C., *et. al.*, the distance from Cα to the unpaired electron which localized to the N-O bond of nitroxide was ~7 Å when MTSSL attached in T4 lysozyme (38).
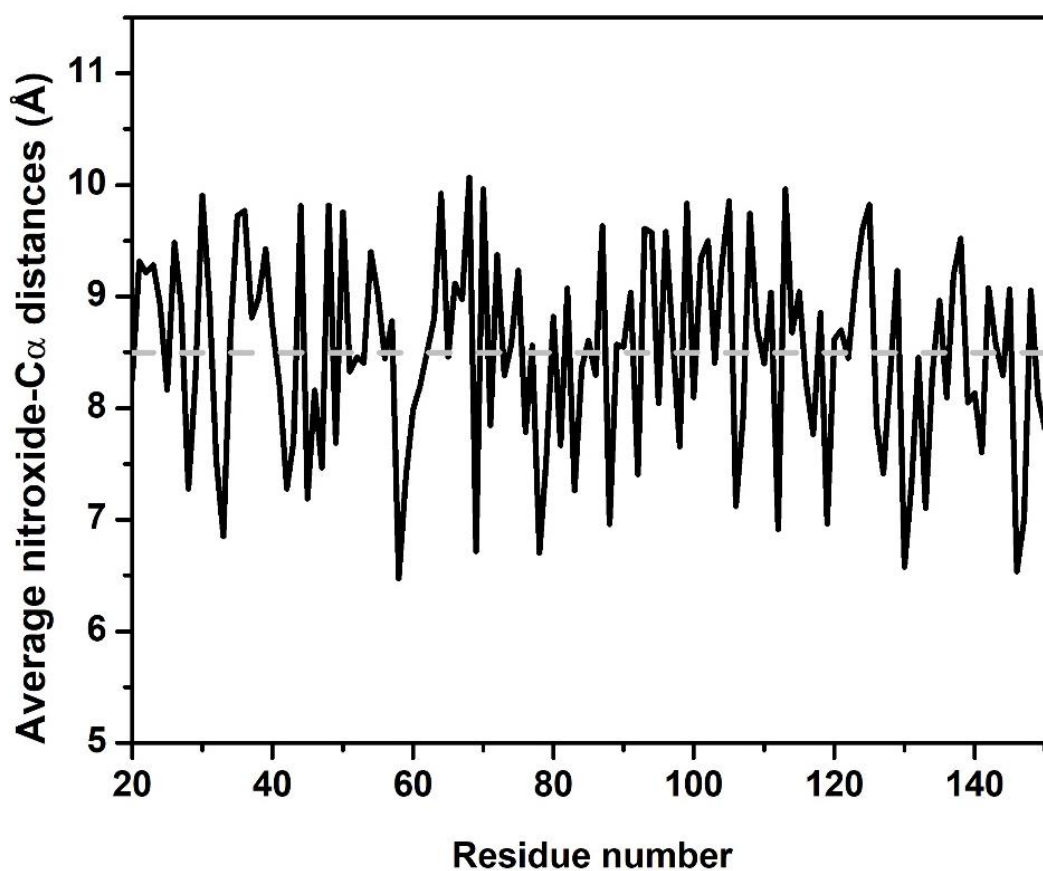
Figure 3.12 Nitroxide-Cα distance variation of all spin labels over the last 1 ns simulation time with average value of 8.5 Å.

3.4   Categories of spin label side chains

To obtain information about surrounding environments of the spin label, the Radial Distribution Function (RDF) plots were generated using the last 2 ns simulations. The environmental RDF analysis over 132 different spin label sites allowed to cluster the spin label side

chain in KvAP-VSD into three categories. These are water-exposed, lipid-exposed and amino acids (protein-buried) spin labels.
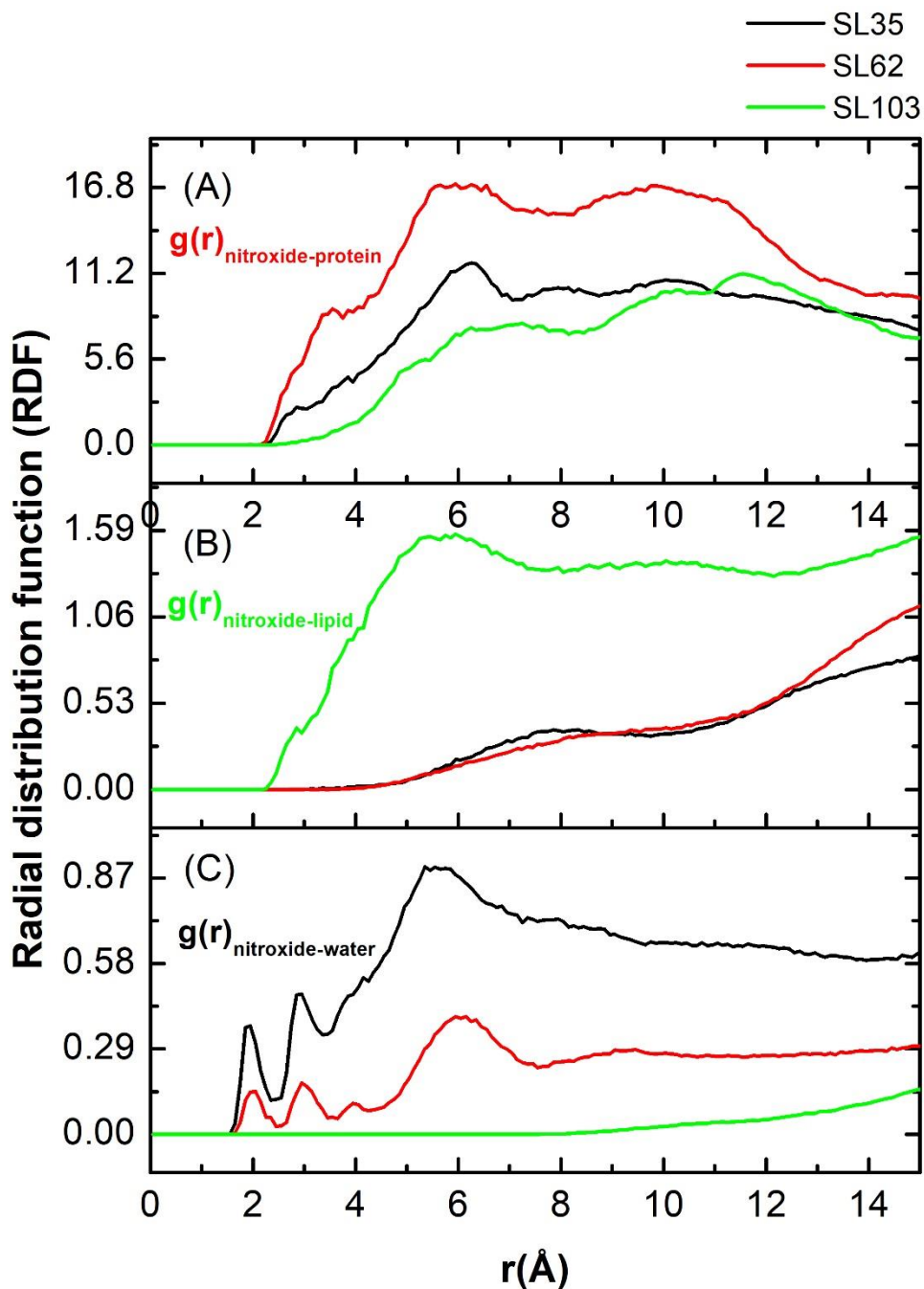
Figure 3.13 Radial distribution function g(r) over the last 2-ns simulations of typical spin label side chains: SL35 (black lines), SL62 (red lines), and SL103 (green lines) in the three different local environments (A) nitroxide-protein, (B) nitroxide-lipid, and (C) nitroxide-water. Atom selections of nitroxide were ON and NN atoms. For water and lipid, atom selections were chains

W and L, respectively. For protein (buried), the protein residues (except two adjacent residues) were selected.

Figure 3.13 shows typical patterns of RDFs for the three neighboring categories of the spin label in KvAP-VSD (SL35, SL62, and SL103). The spin label of SL35 (black lines) was exposed to water as shown by the first peak of the spin label-water RDF at a distance of about 2 Å while that of SL103 (green lines) was exposed to lipid at around 6 Å distance. The spin label of SL62 was found to be buried inside the protein by orienting towards the central core of VSD (Figure 3.14). However, it also contacts with water molecules as indicated by a peak of the RDF of spin label-water at ~2 Å. This suggested that water molecules were accessible into the VSD core during the simulations. The results were consistent with experimental and simulation data reported previously.

SL35   **SL62**   **SL103**
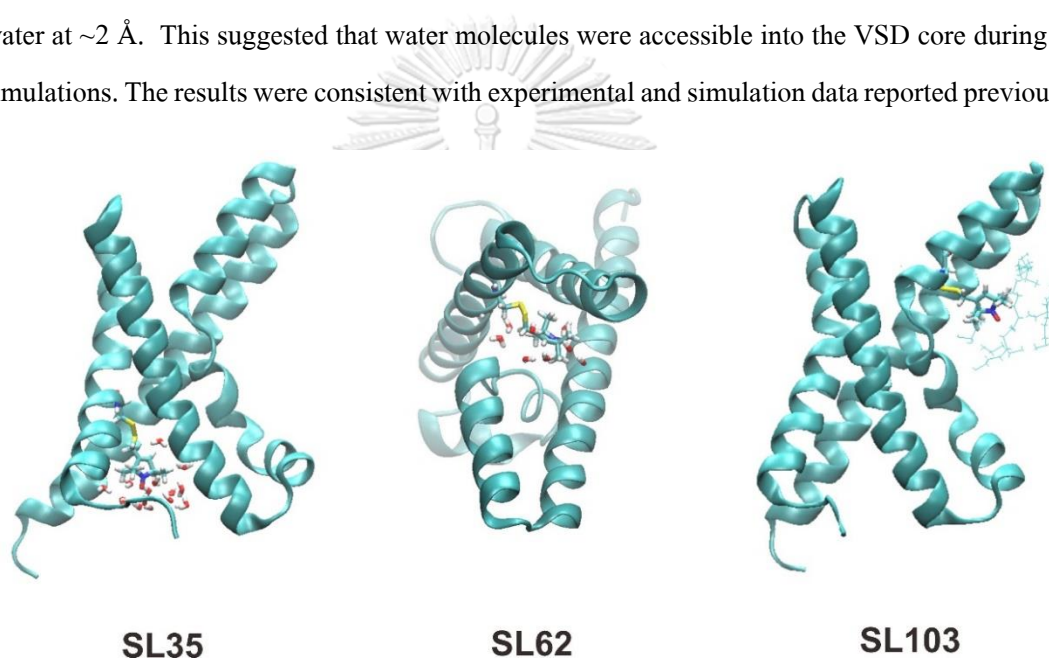
Figure 3.14 Spin label side chains in their different immediate environments: SL35 (water-exposed), SL62 (buried), and SL103 (lipid-exposed)
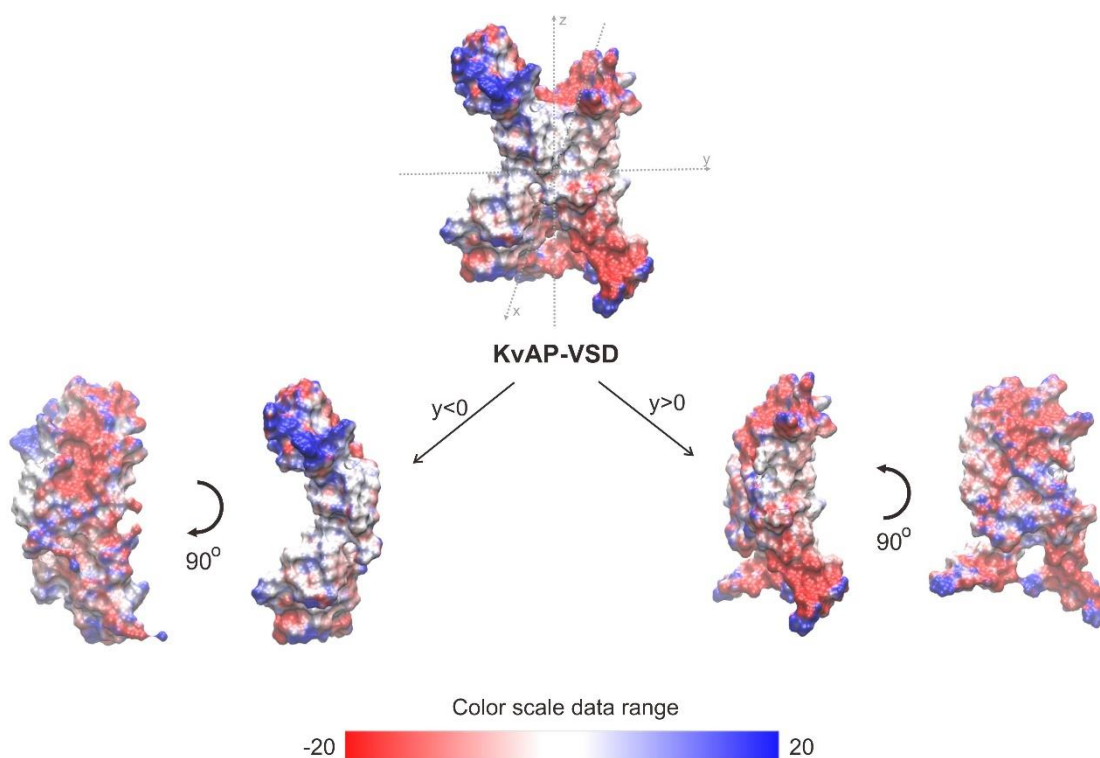
The Poisson-Boltzmann electrostatic potential molecular surface of KvAP-VSD was determined using APBS (Adaptive Poisson-Boltzmann Solver) program and demonstrated in Figure 3.15. Red represented areas of the most negative electrostatic potential. The most positive electrostatic potential regions were represented by blue. White represented zero potential regions. Potential increases in the order red < white < blue. More polar the molecule was, larger red/blue differences appeared. For nonpolar areas, the surface had brighter shades. In Figure 3.15, therefore, it is obvious that water molecules are able to penetrate into the VSD hole and then interact with the spin label side chains.

KvAP-VSD

Figure 3.15 Molecular surface of KvAP-VSD mapped using Poisson-Boltzmann electrostatic potential

Table 3.4 Average RMSF and mobility of each category of spin label side chains

Type	Water exposed	Lipid exposed	Buried
RMSF (Å)	0.97	0.88	0.84
Mobility (g^{-1})	0.24	0.22	0.21

The average RMSF and mobility of each spin label side-chain group were calculated and shown in Table 3.4. Additionally, we constructed the distribution RMSF and mobility data for each spin label category using box plots as in Figure 3.16 and 3.17. In both graphs, the water-exposed spin label side chains were more flexible than the lipid-exposed ones while the buried spin labels had the slowest motions. The correlation between the normalized values of the average RMSF and mobility for each group of sin label side chains was identified and expressed in Figure 3.18. The square of the correlation value (R^2) was equal to 0.9994, implying that the dynamical properties of characterized spin label sites in the protein highly consistent with the experimental EPR data. The

drawback of this approach is that some spin label side chains can expose to two environments at the same time (interface regions).
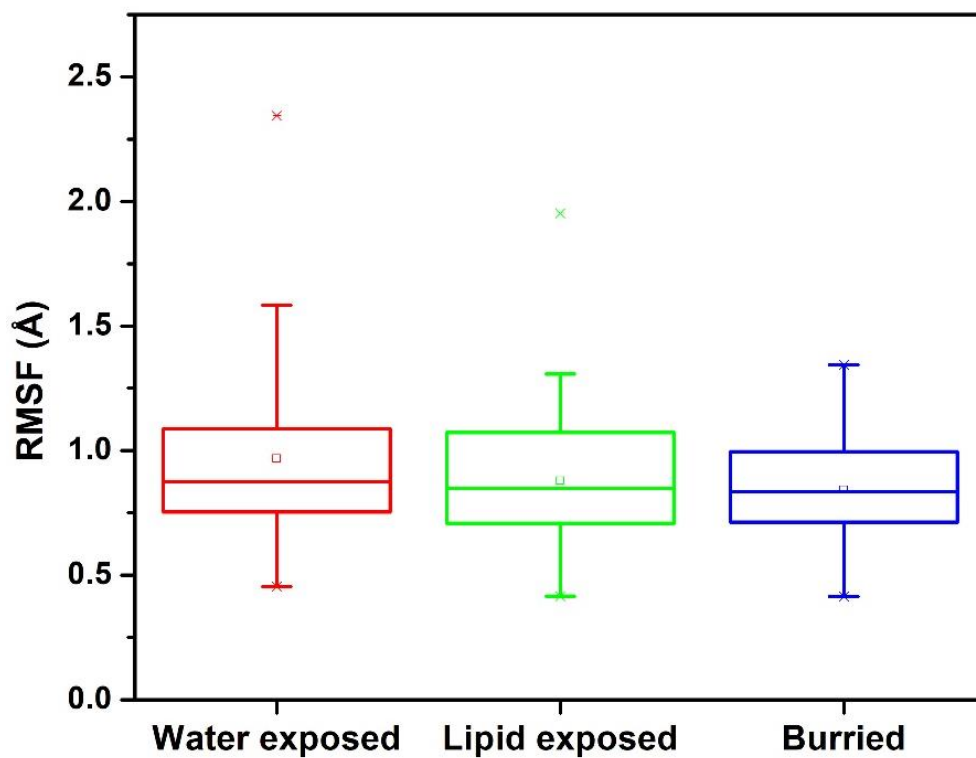
Figure 3.16 RMSF box plot of each category of spin label side chains: water-exposed (red box), lipid-exposed (green box), and buried (blue box)
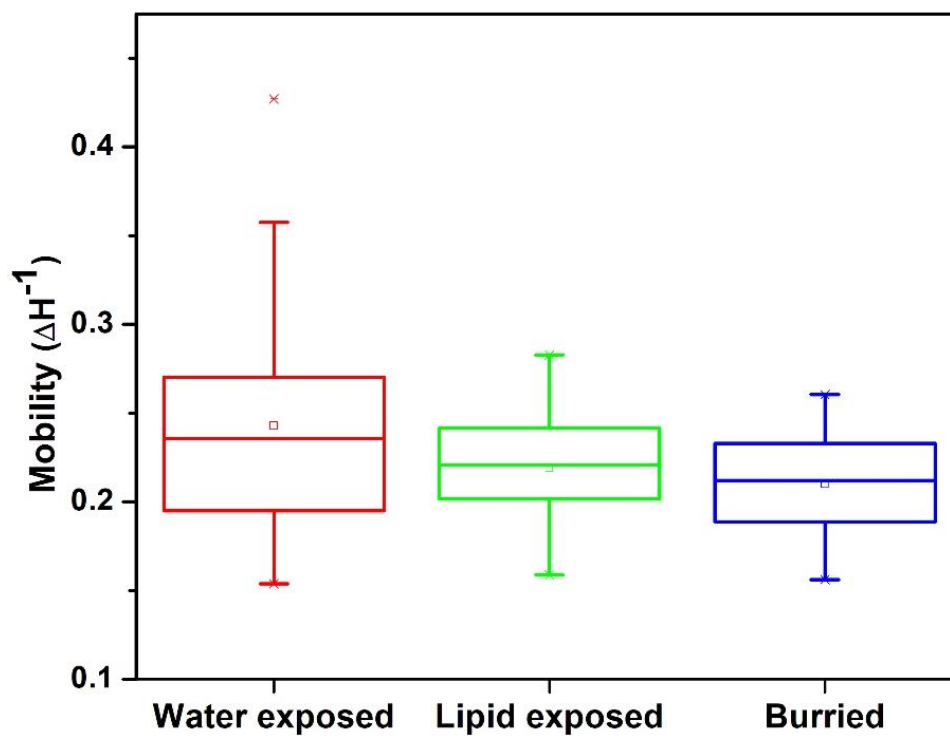
Figure 3.17 Mobility box plot of each category of spin label side chains: water-exposed (red box), lipid-exposed (green box), and buried (blue box)
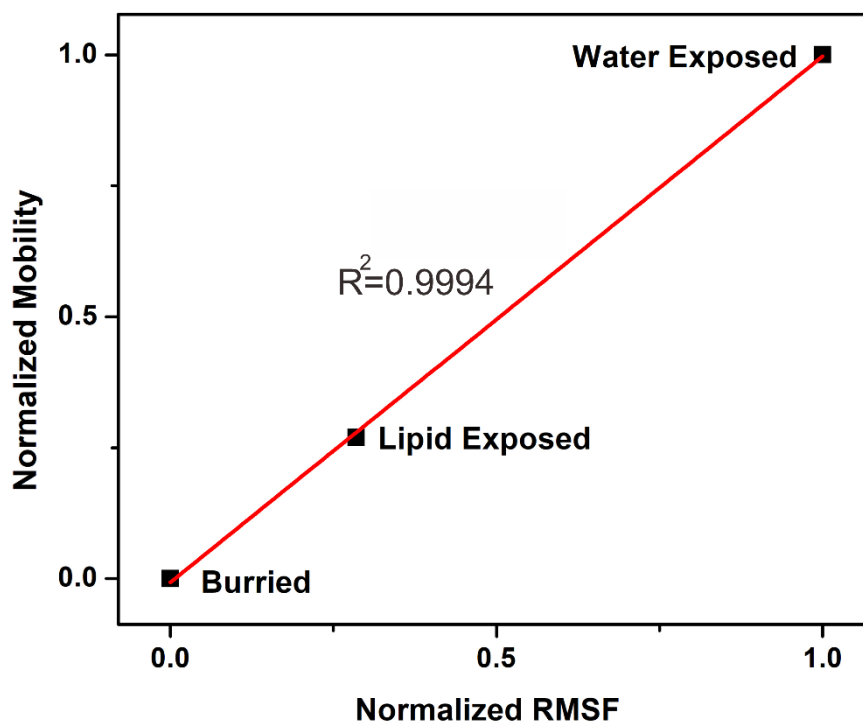

Figure 3.18 Correlation plot of the RMSF and mobility data of spin label categories

Chapter 4

CONCLUSIONS

We constructed structures of the cysteine-mutated membrane protein with the nitroxide spin label attaching at 132 positions (residues 20-151) of the KvAP voltage sensor domain (VSD), using CHARMM-GUI and VMD. Next, all-atom MD simulations were performed over 10 ns for all systems, then analyzing MD trajectories. Root-mean-square fluctuation (RMSF) of each spin label side-chain was calculated and compared with the experimental mobility data. The spin label side chains attached in the loops were more flexible than those in the segments, which was well consistent with the experimental EPR data.

Importantly, it was found that owing to the similar pattern in RMSF plots, the mobility of the spin label side-chain can be used to reflect the backbone dynamics. The conformational fluctuations of spin label side chains were represented by the dihedral angle distribution and the variation of the nitroxide-Cα distances. Moreover, the categories of the spin label side chains based on the local environments were also established using radial distribution function (RDF) method. Besides, the dynamics of the spin label side chains were decreased in the order water-exposed > lipid-exposed > buried type.

Dihedral angles of all spin label side chains 20-151: χ_1 (blue), χ_2 (red), χ_3 (yellow), χ_4 (purple), and χ_5 (green)
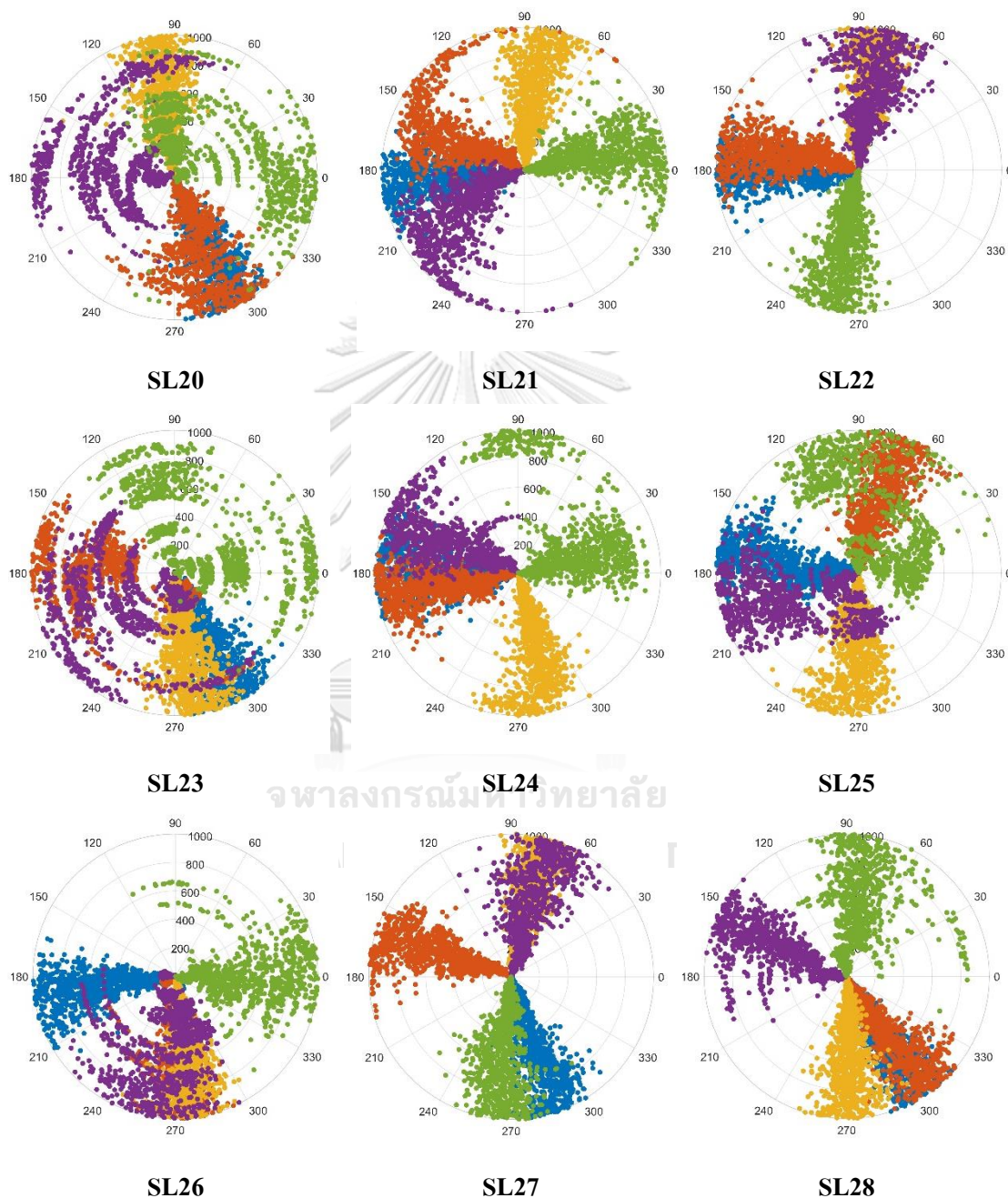
Figure 1S.1 Dihedral angles of R1 side chains over the last 1 ns MD trajectory (SL20-28)
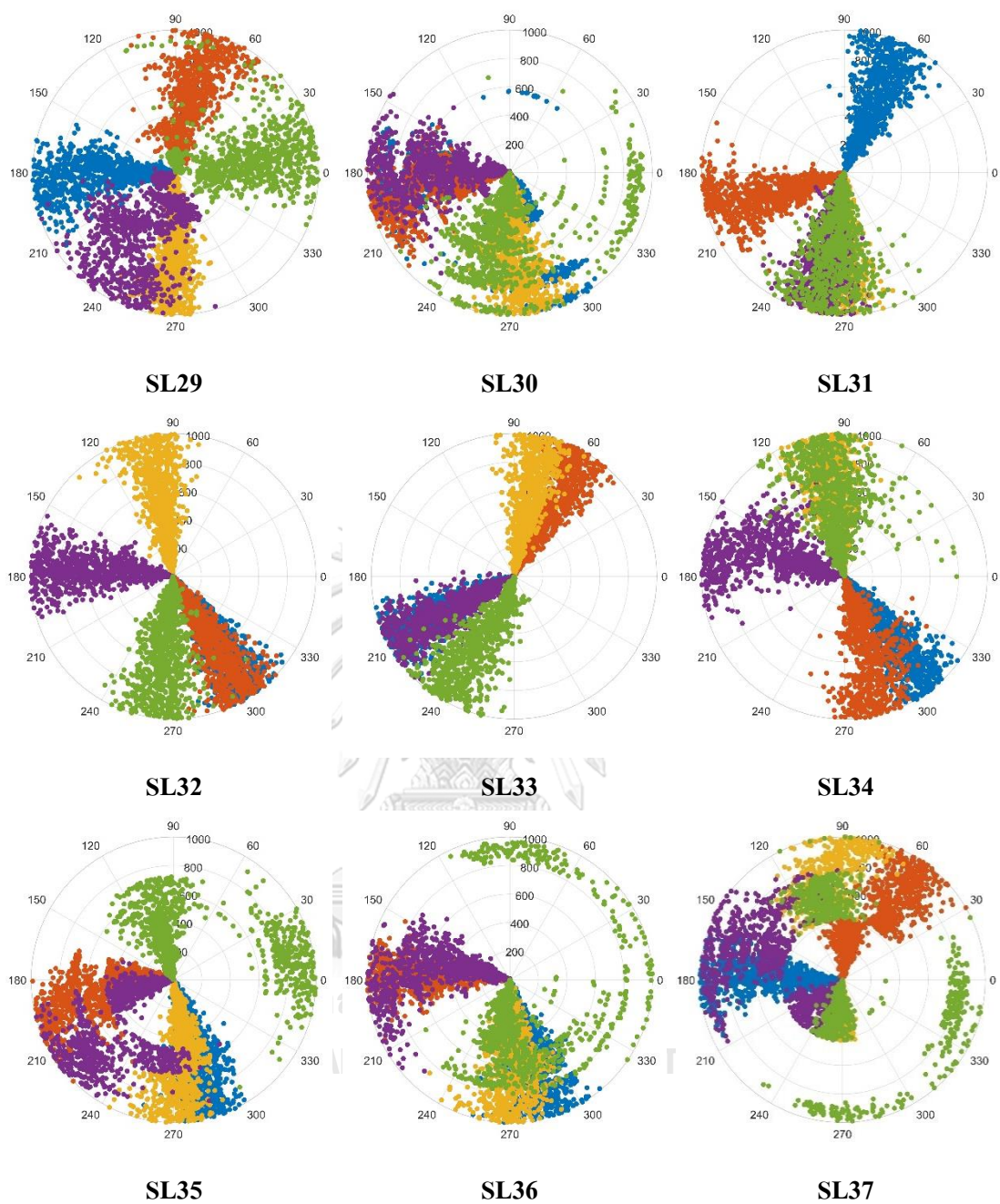
Figure 1S.2 Dihedral angles of R1 side chains over the last 1 ns MD trajectory (SL29-37)
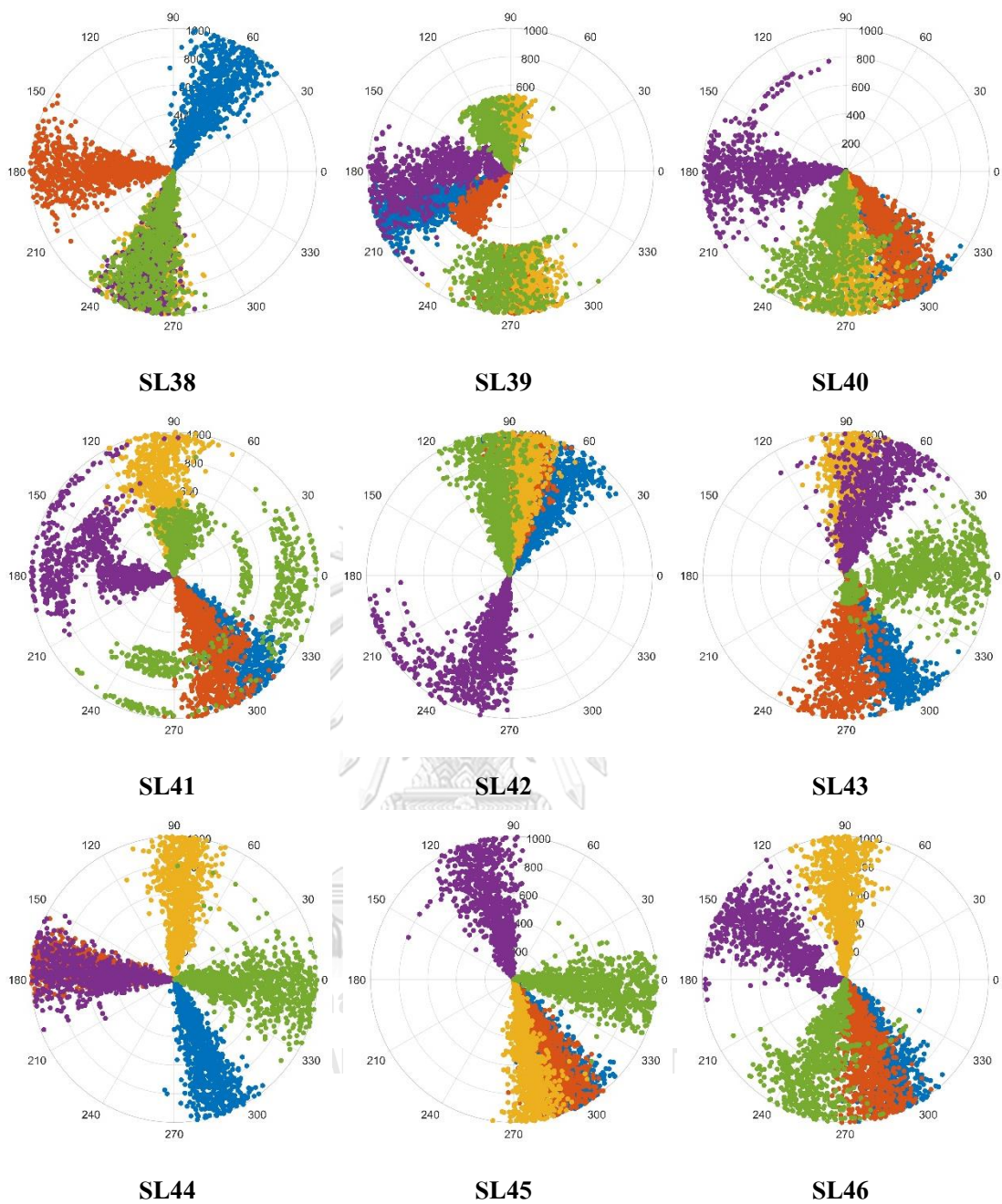
Figure 1S.3 Dihedral angles of R1 side chains over the last 1 ns MD trajectory (SL38-46)

SL47

SL48

SL49

SL50

SL51

SL52

SL53

SL54

SL55

Figure 1S.4 Dihedral angles of R1 side chains over the last 1 ns MD trajectory (SL47-55)

Figure 1S.5 Dihedral angles of R1 side chains over the last 1 ns MD trajectory (SL56-64)

SL65   **SL66**   **SL67**

SL68   **SL69**   **SL70**

SL71   **SL72**   **SL73**

Figure 1S.6 Dihedral angles of R1 side chains over the last 1 ns MD trajectory (SL65-73)

SL74

SL75

SL76

SL77

SL78

SL79

SL80

SL81

SL82

Figure 1S.7 Dihedral angles of R1 side chains over the last 1 ns MD trajectory (SL74-82)

Figure 1S.8 Dihedral angles of R1 side chains over the last 1 ns MD trajectory (SL83-91)

Figure 1S.9 Dihedral angles of R1 side chains over the last 1 ns MD trajectory (SL92-100)

Figure 1S.10 Dihedral angles of R1 side chains over the last 1 ns MD trajectory (SL101-109)

Figure 1S.11 Dihedral angles of R1 side chains over the last 1 ns MD trajectory (SL110-118)

Figure 1S.12 Dihedral angles of R1 side chains over the last 1 ns MD trajectory (SL119-127)
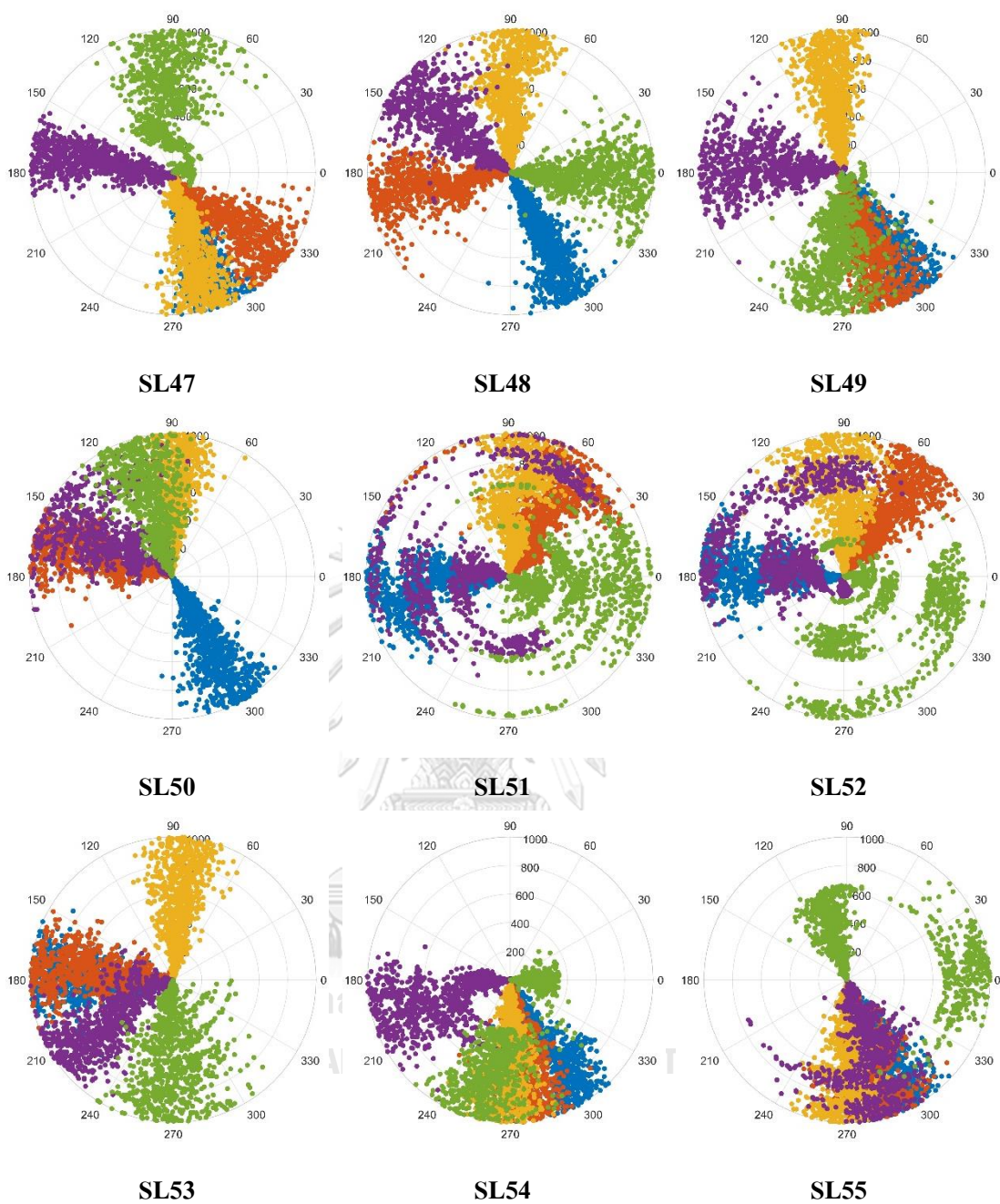
Figure 1S.13 Dihedral angles of R1 side chains over the last 1 ns MD trajectory (SL128-136)
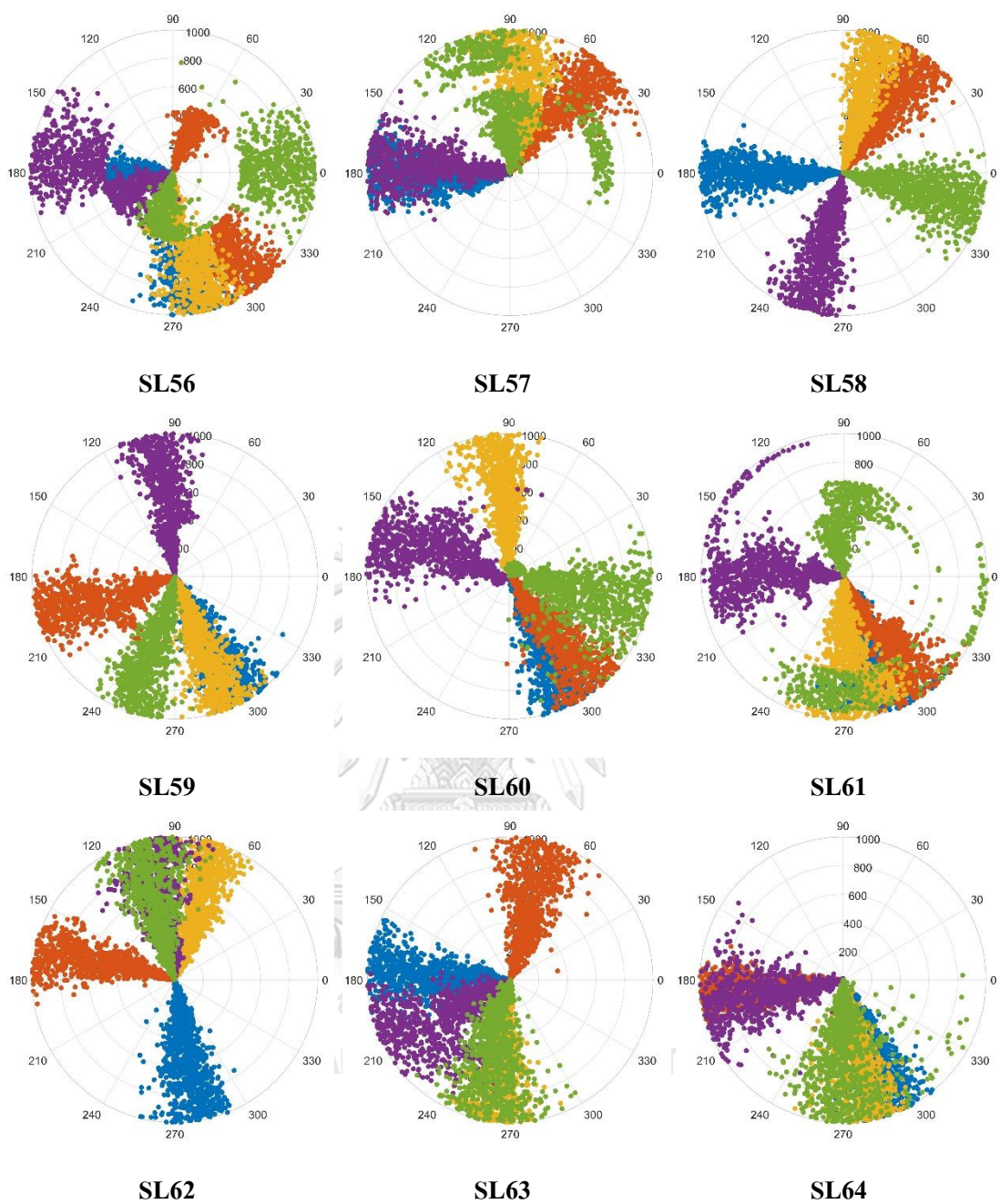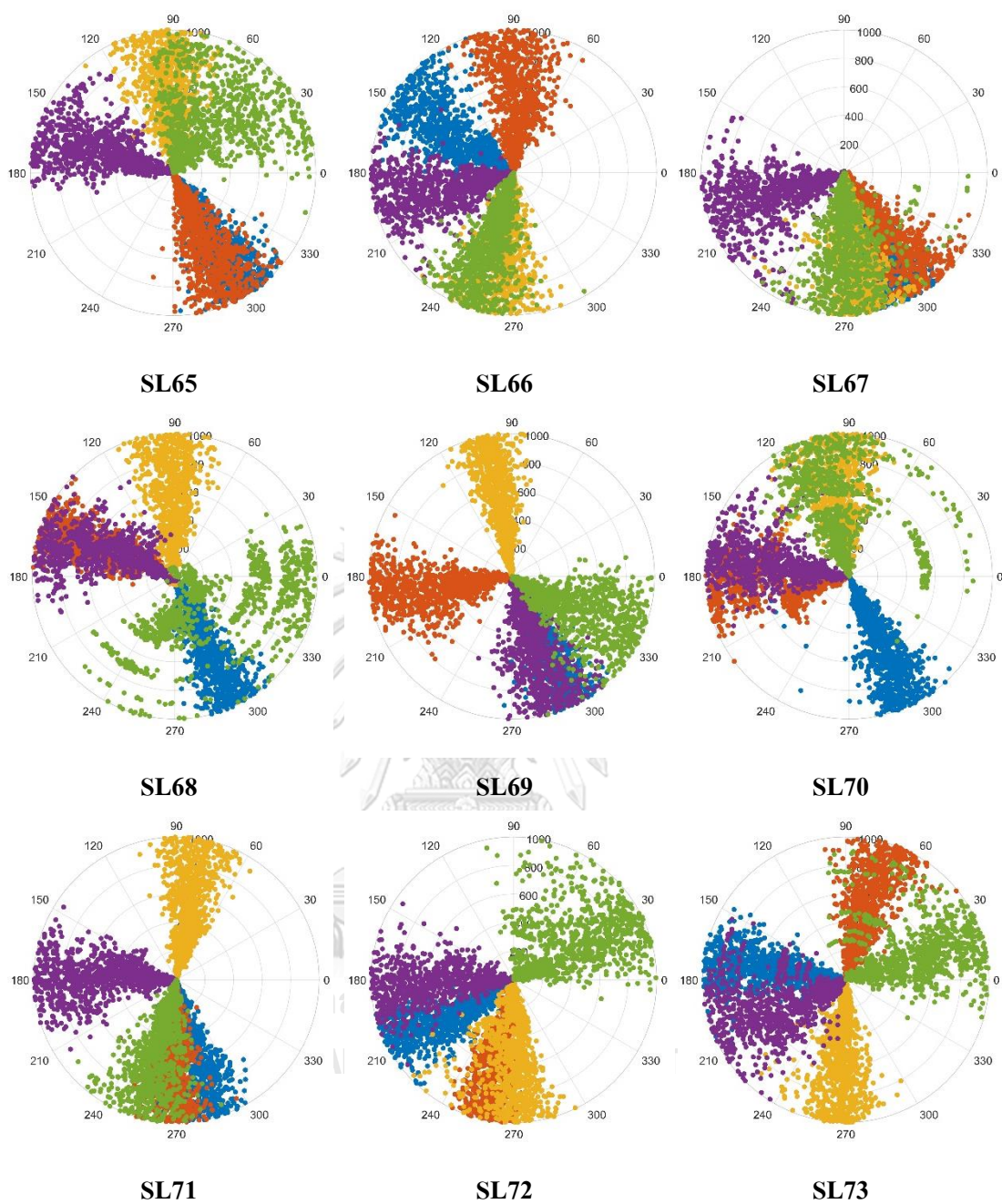
Figure 1S.14 Dihedral angles of R1 side chains over the last 1 ns MD trajectory (SL137-145)
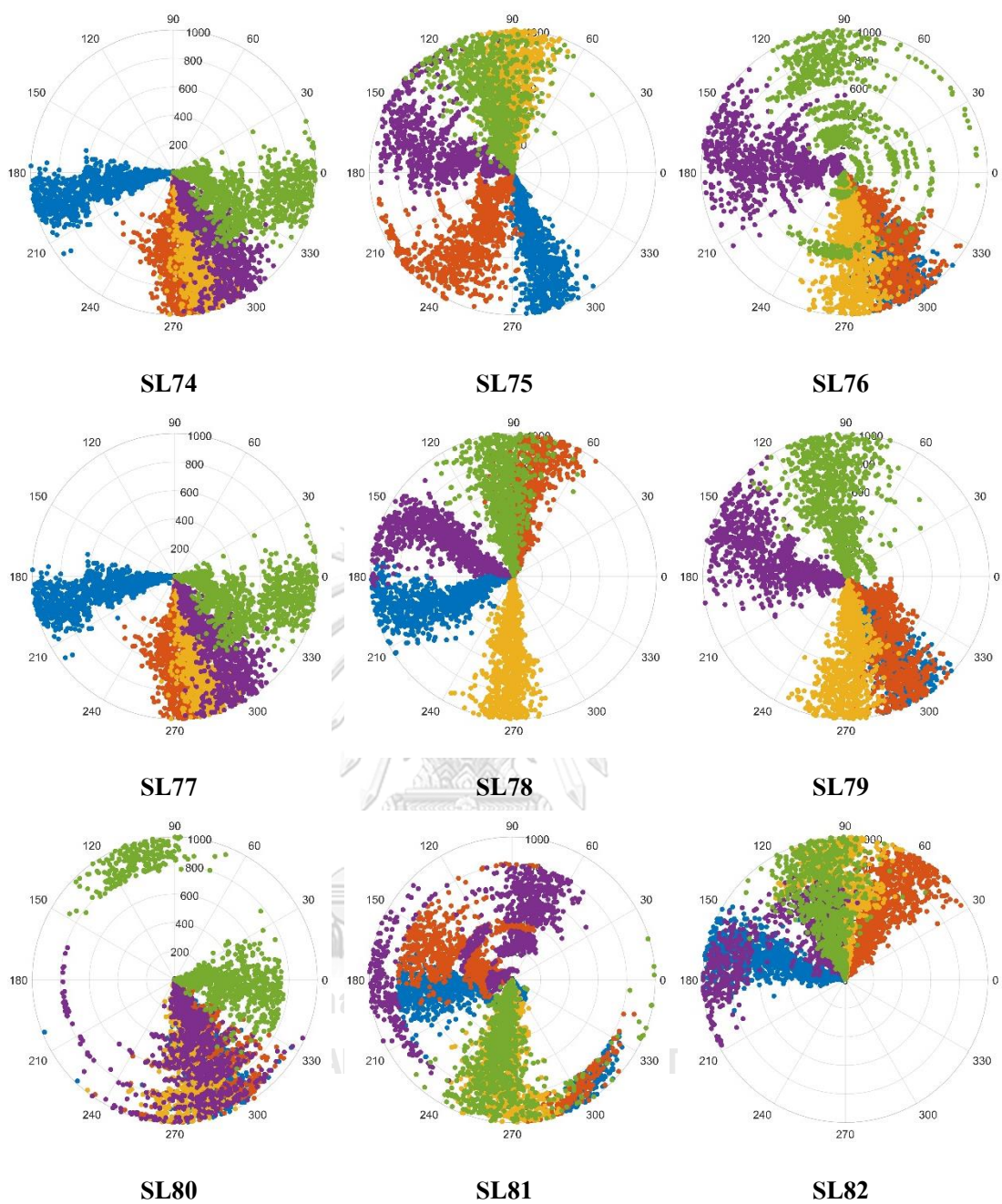
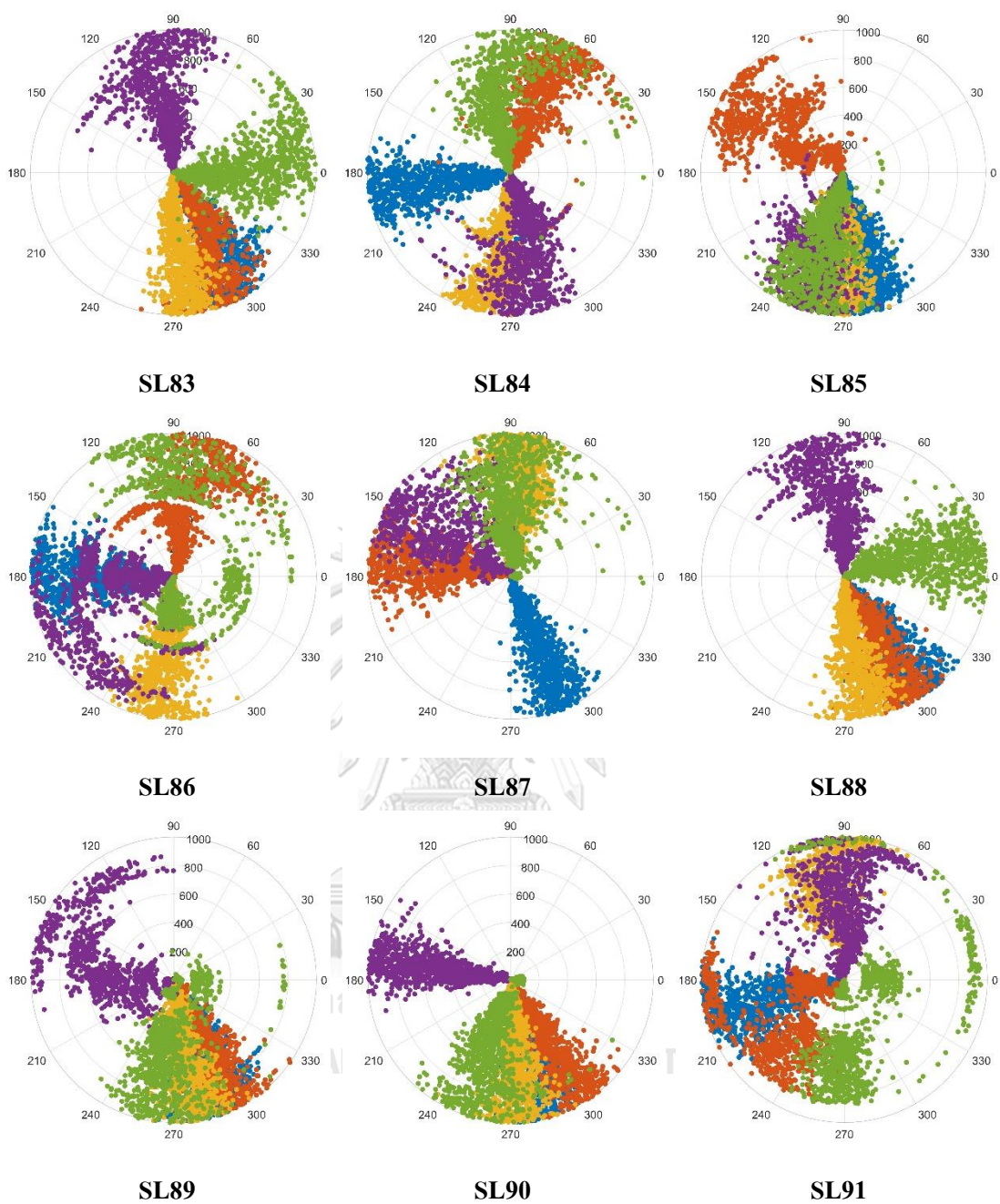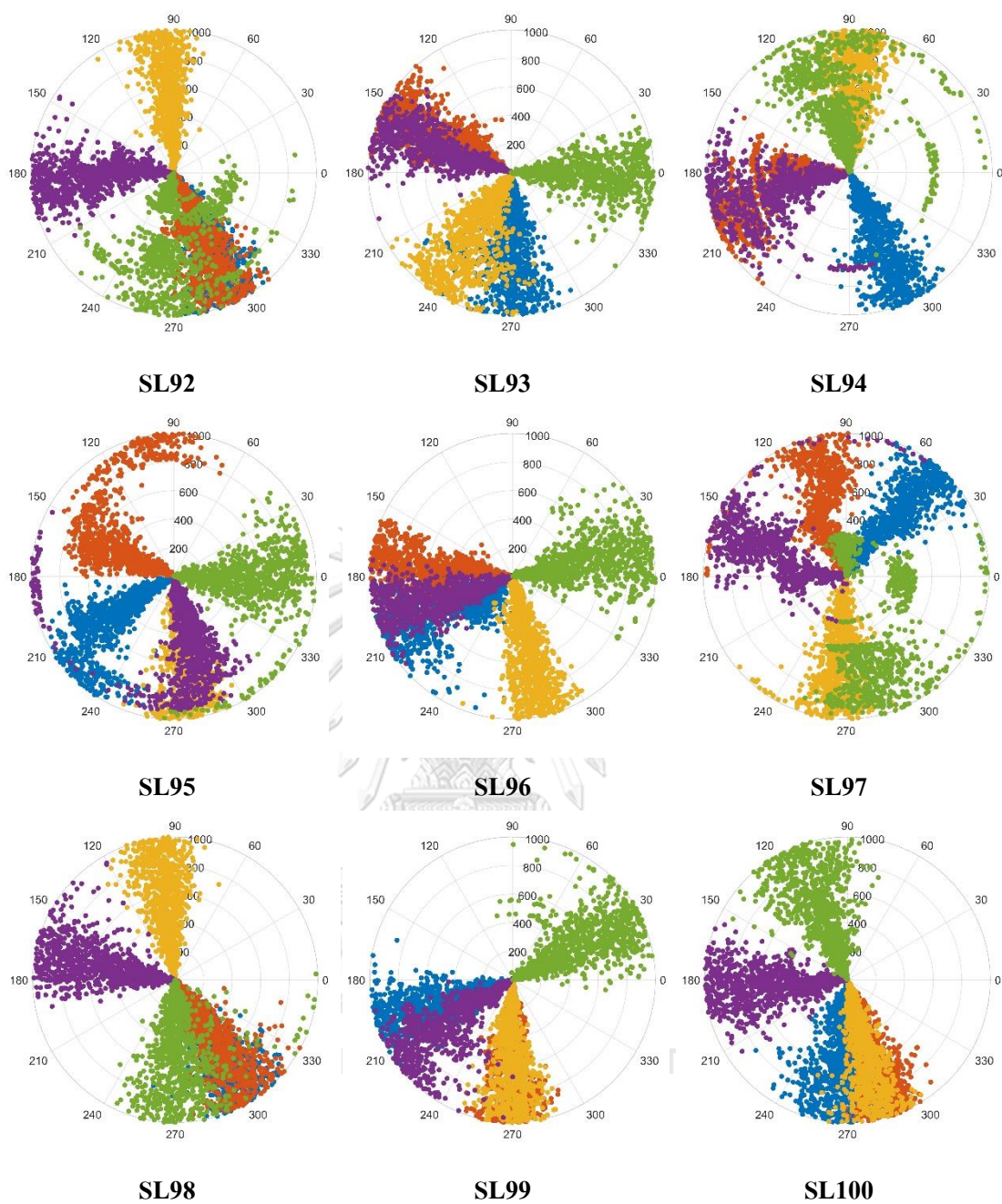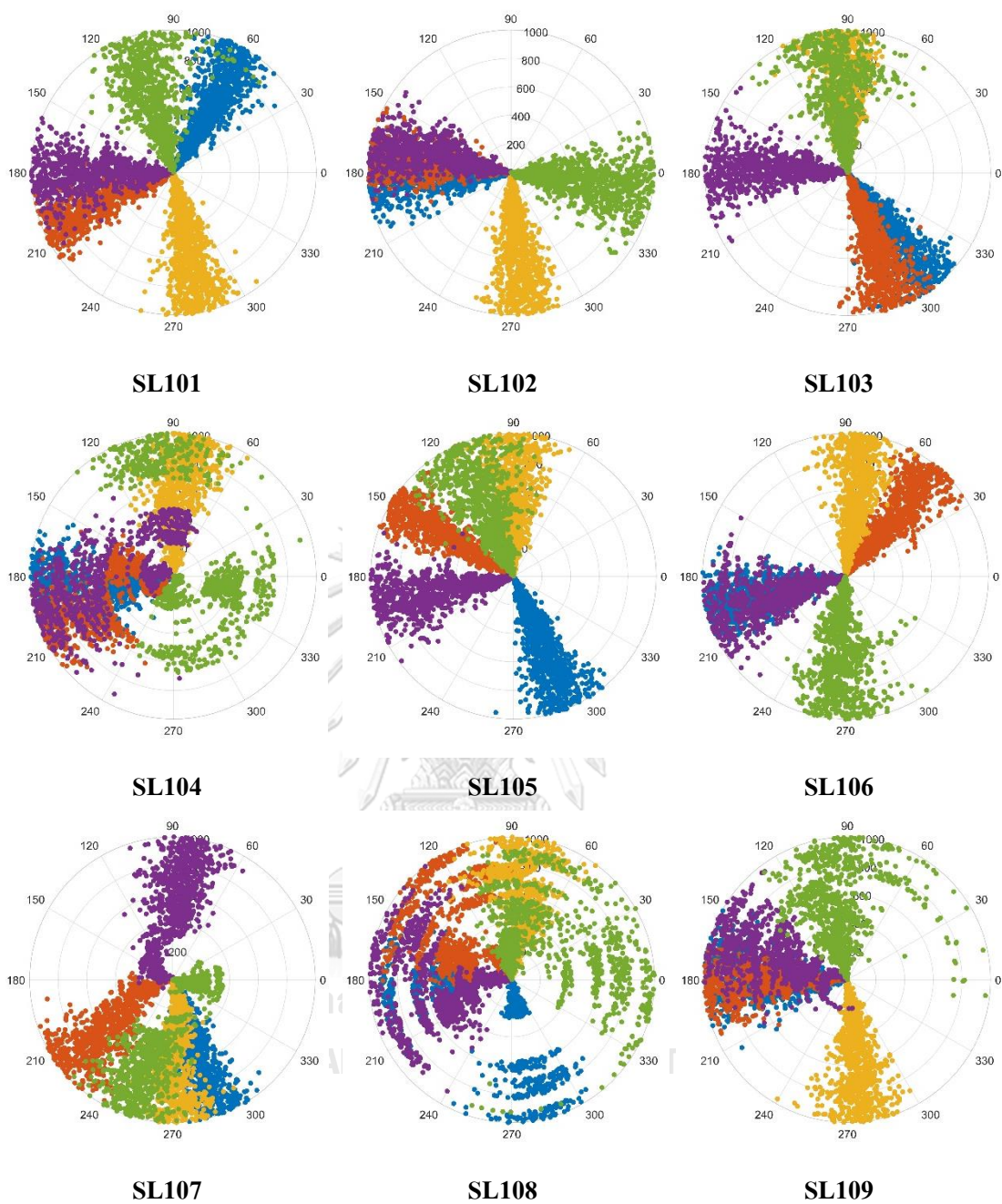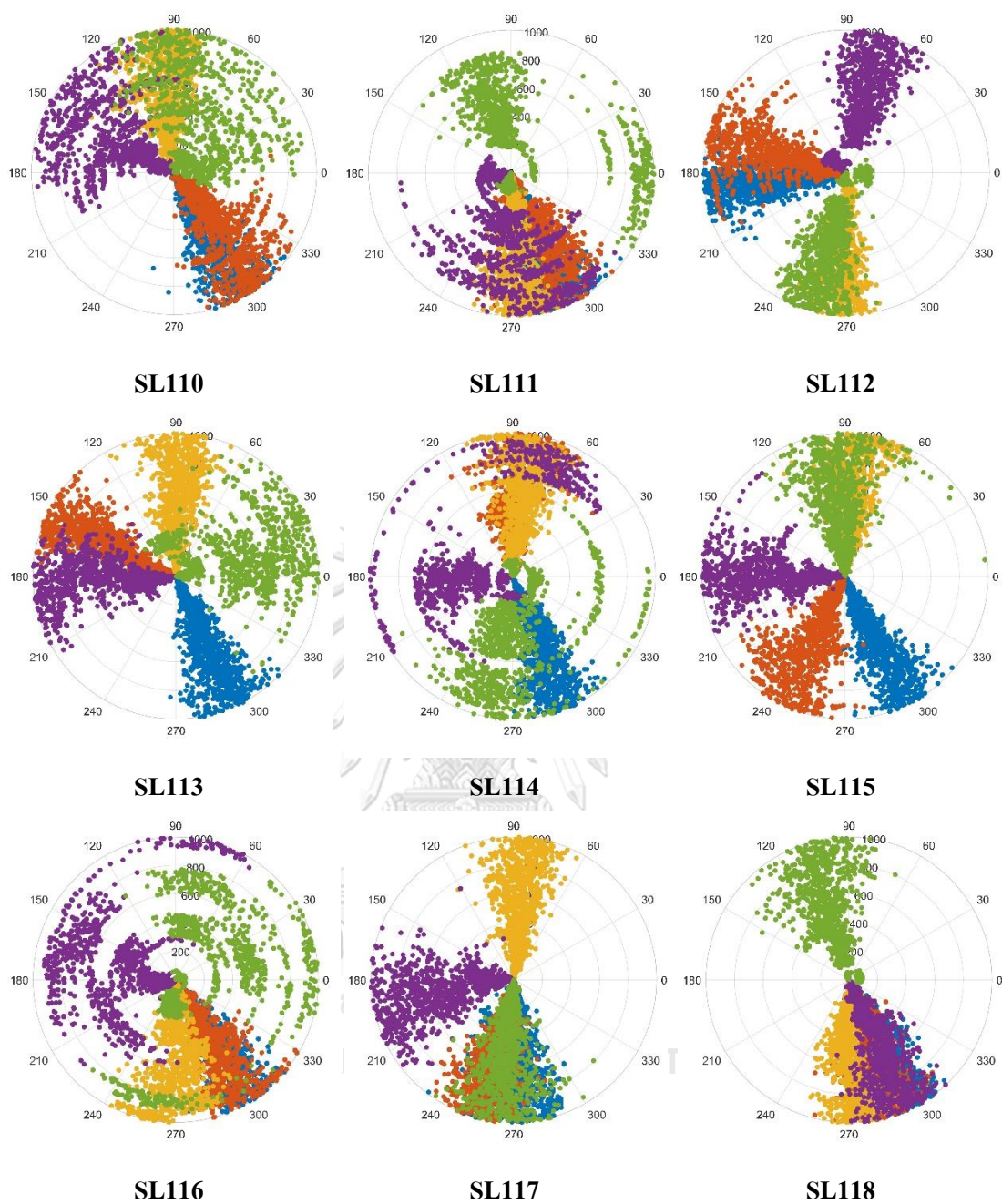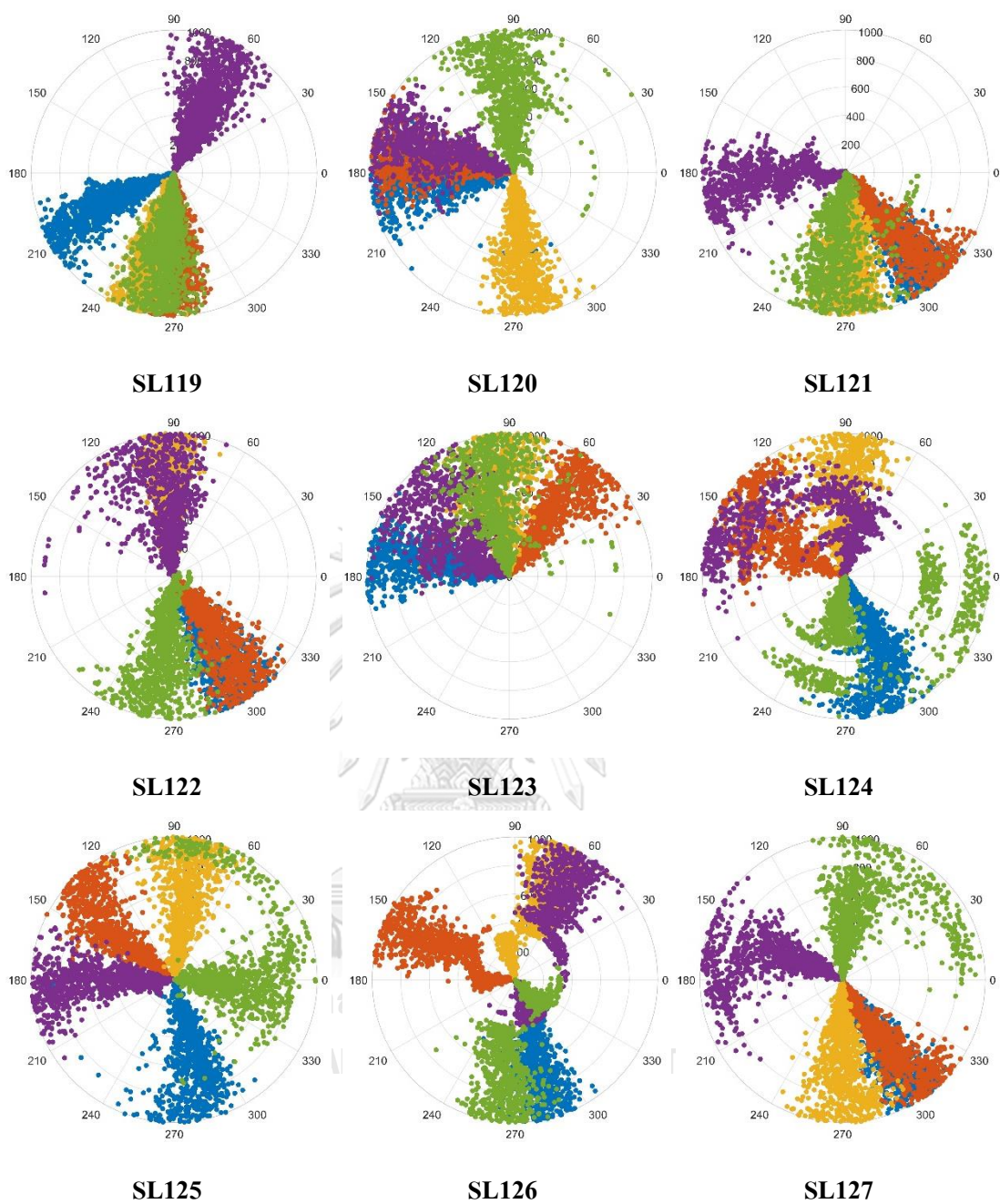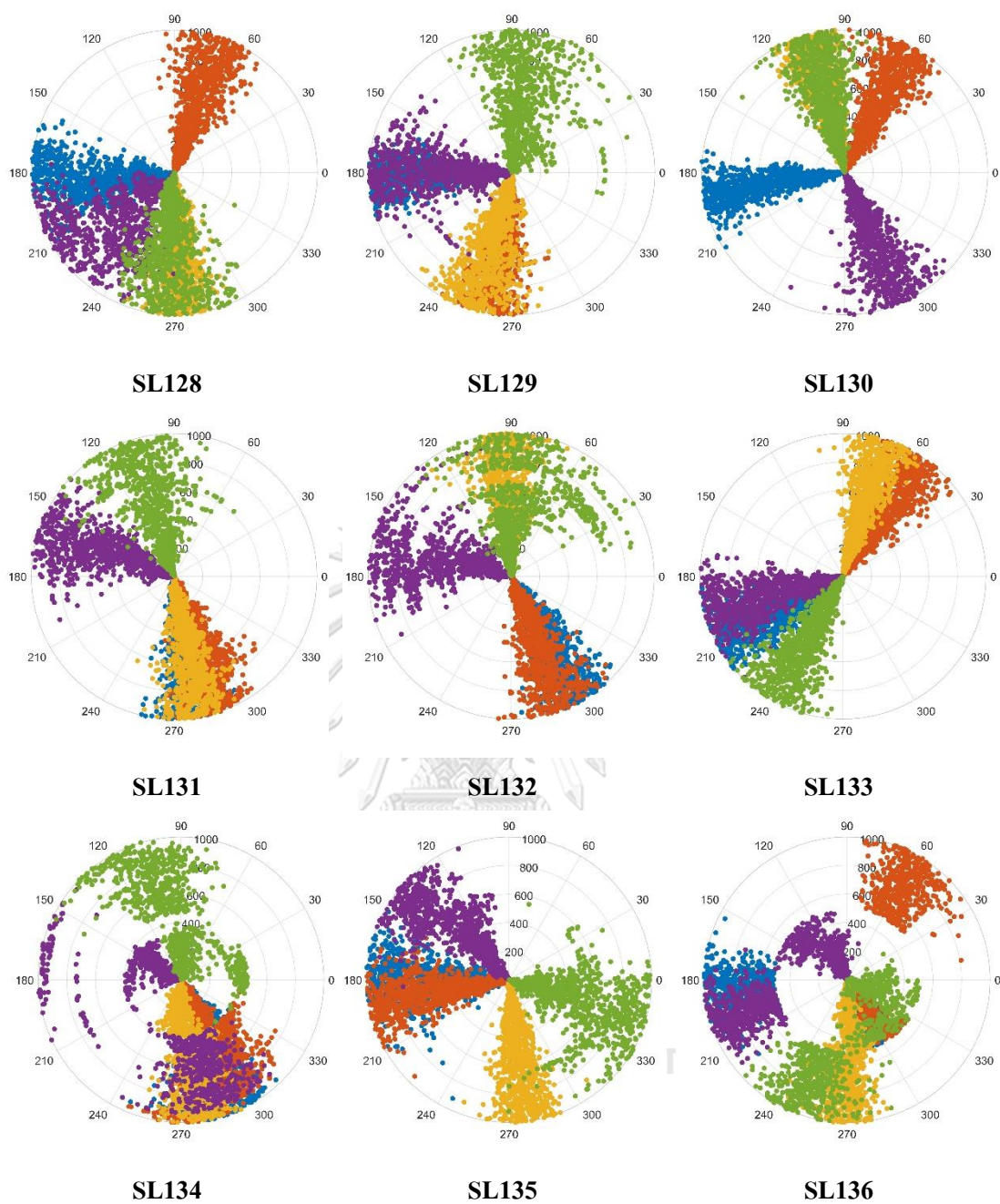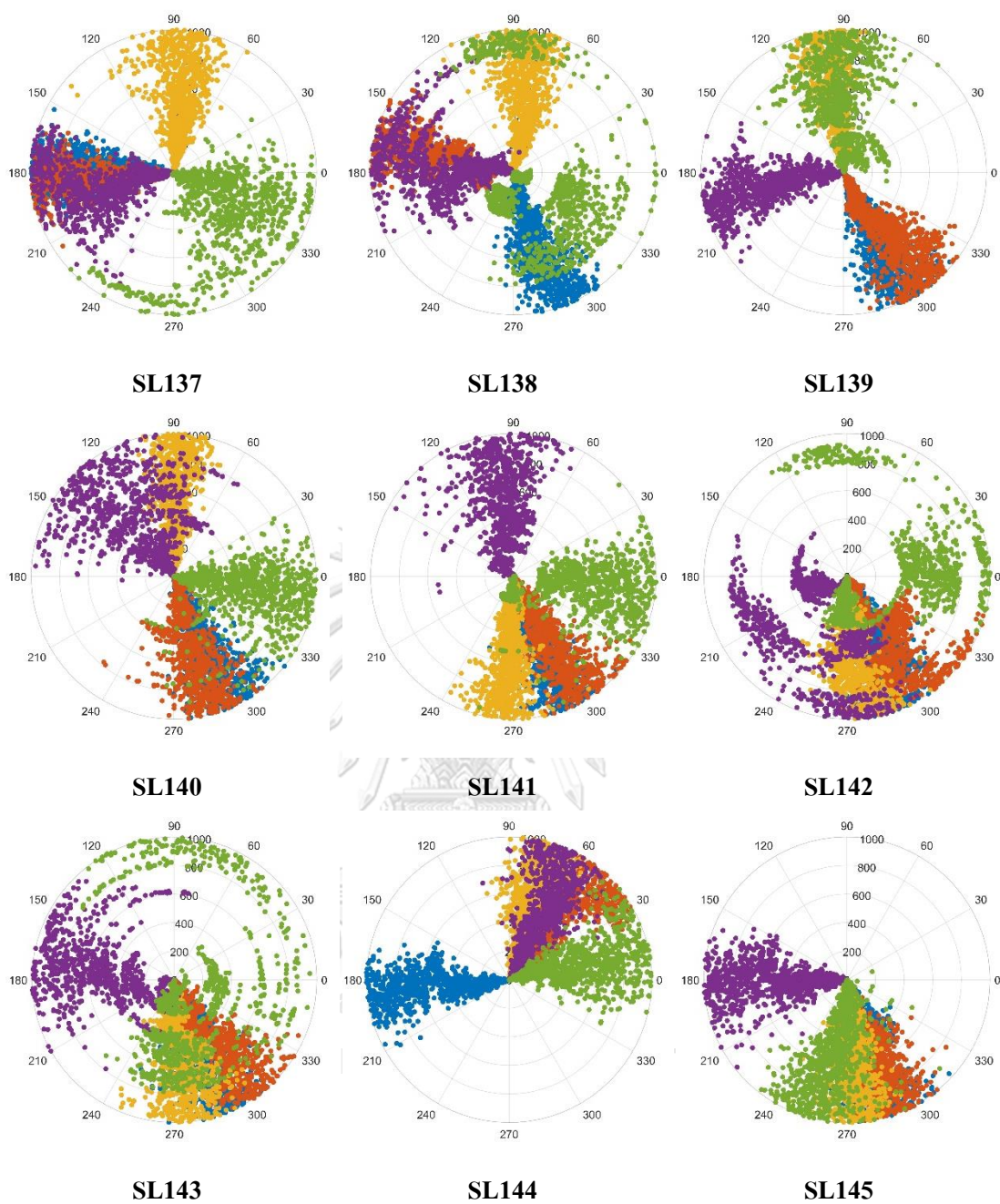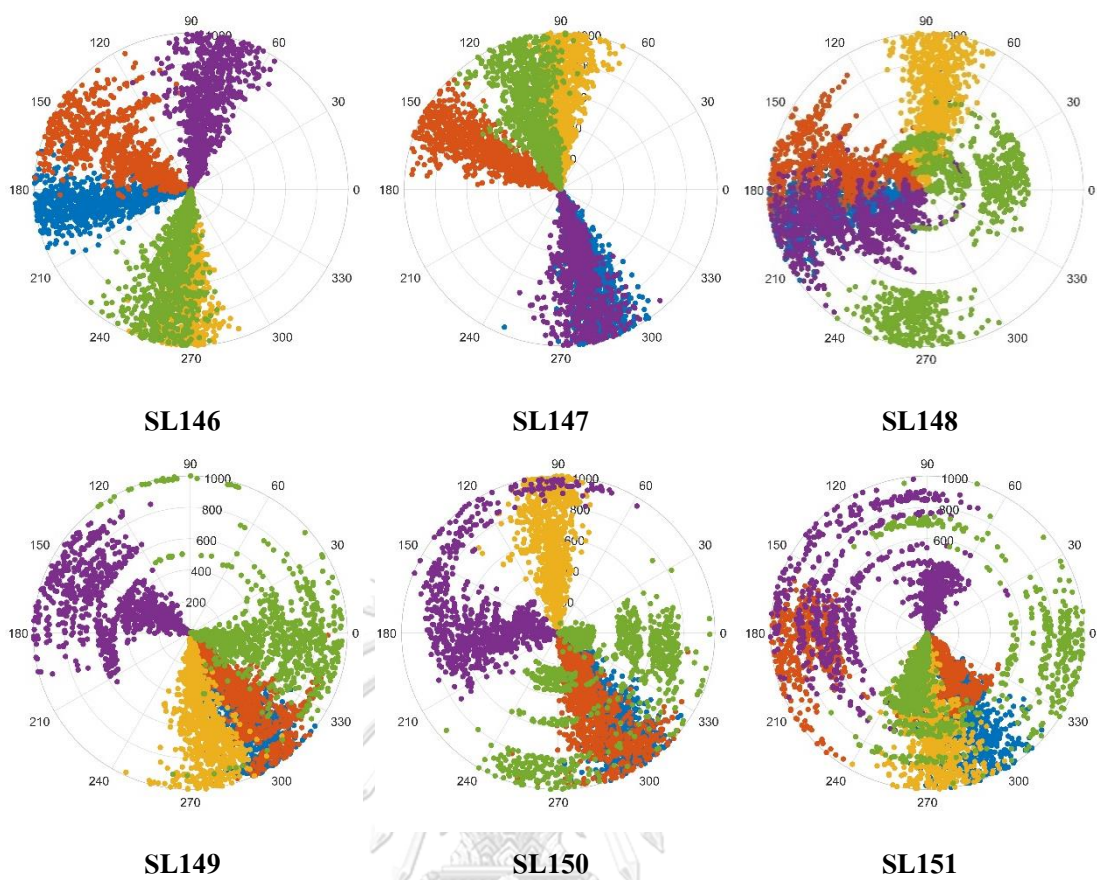**Figure 1S.15** Dihedral angles of R1 side chains over the last 1 ns MD trajectory (SL146-151)
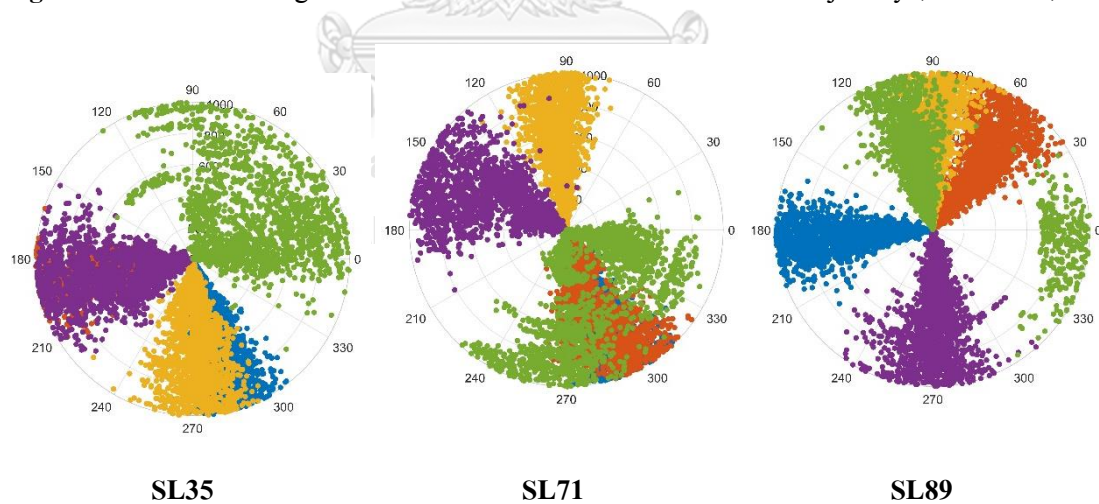
Figure 2S. Dihedral angles of R1 side chains (SL35, SL71, and SL89) over the last 1 ns of 100-ns MD simulation

REFERENCES

1. Goossens, K., and De Winter, H. (2018) Molecular Dynamics Simulations of Membrane Proteins: An Overview. *J Chem Inf Model* **58**, 2193-2202

2. von Heijne, G. (2007) The membrane protein universe: what's out there and why bother? *J Intern Med* **261**, 543-557

3. Overington, J. P., Al-Lazikani, B., and Hopkins, A. L. (2006) How many drug targets are there? *Nat Rev Drug Discov* **5**, 993-996

4. Cornish, V. W., Benson, D. R., Altenbach, C. A., Hideg, K., Hubbell, W. L., and Schultz, P. G. (1994) Site-specific incorporation of biophysical probes into proteins. *Proc Natl Acad Sci U S A* **91**, 2910-2914

5. Klare, J. P., and Steinhoff, H. J. (2009) Spin labeling EPR. *Photosynth Res* **102**, 377-390

6. Sahu, I. D., and Lorigan, G. A. (2018) Site-Directed Spin Labeling EPR for Studying Membrane Proteins. *Biomed Res Int* **2018**, 3248289

7. Balo, A. R., Feyrer, H., and Ernst, O. P. (2016) Toward Precise Interpretation of DEER-Based Distance Distributions: Insights from Structural Characterization of V1 Spin-Labeled Side Chains. *Biochemistry* **55**, 5256-5263

8. Fielding, A. J., Concilio, M. G., Heaven, G., and Hollas, M. A. (2014) New developments in spin labels for pulsed dipolar EPR. *Molecules* **19**, 16998-17025

9. Hubbell, W. L., Lopez, C. J., Altenbach, C., and Yang, Z. (2013) Technological advances in site-directed spin labeling of proteins. *Curr Opin Struct Biol* **23**, 725-733

10. Roser, P., Schmidt, M. J., Drescher, M., and Summerer, D. (2016) Site-directed spin labeling of proteins for distance measurements in vitro and in cells. *Org Biomol Chem* **14**, 5468-5476

11. Sahu, I. D., McCarrick, R. M., and Lorigan, G. A. (2013) Use of electron paramagnetic resonance to solve biochemical problems. *Biochemistry* **52**, 5967-5984

12. Sahu, I. D., McCarrick, R. M., Troxel, K. R., Zhang, R., Smith, H. J., Dunagan, M. M., Swartz, M. S., Rajan, P. V., Kroncke, B. M., Sanders, C. R., and Lorigan, G. A. (2013) DEER EPR measurements for membrane protein structures via bifunctional spin labels and lipodisq nanoparticles. *Biochemistry* **52**, 6627-6632

13. Schreier, S., Bozelli, J. C., Jr., Marin, N., Vieira, R. F., and Nakaie, C. R. (2012) The spin label amino acid TOAC and its uses in studies of peptides: chemical, physicochemical, spectroscopic, and conformational aspects. *Biophys Rev* **4**, 45-66

14. Stoller, S., Sicoli, G., Baranova, T. Y., Bennati, M., and Diederichsen, U. (2011) TOPP: a novel nitroxide-labeled amino acid for EPR distance measurements. *Angew Chem Int Ed Engl* **50**, 9743-9746

15. Ruta, V., Jiang, Y., Lee, A., Chen, J., and MacKinnon, R. (2003) Functional analysis of an archaebacterial voltage-dependent K+ channel. *Nature* **422**, 180-185

16. Li, Q., Wanderling, S., Sompornpisut, P., and Perozo, E. (2014) Structural basis of lipid-driven conformational transitions in the KvAP voltage-sensing domain. *Nat Struct Mol Biol* **21**, 160-166

17. Altenbach, C., Marti, T., Khorana, H. G., and Hubbell, W. L. (1990) Transmembrane protein structure: spin labeling of bacteriorhodopsin mutants. *Science* **248**, 1088-1092

18. Columbus, L., and Hubbell, W. L. (2002) A new spin on protein dynamics. *Trends Biochem Sci* **27**, 288-295

19. Columbus, L., Kalai, T., Jeko, J., Hideg, K., and Hubbell, W. L. (2001) Molecular motion of spin labeled side chains in alpha-helices: analysis by variation of side chain structure. *Biochemistry* **40**, 3828-3846

20. Fleissner, M. R., Bridges, M. D., Brooks, E. K., Cascio, D., Kalai, T., Hideg, K., and Hubbell, W. L. (2011) Structure and dynamics of a conformationally constrained nitroxide side chain and applications in EPR spectroscopy. *Proc Natl Acad Sci U S A* **108**, 16241-16246

21. Fleissner, M. R., Brustad, E. M., Kalai, T., Altenbach, C., Cascio, D., Peters, F. B., Hideg, K., Peuker, S., Schultz, P. G., and Hubbell, W. L. (2009) Site-directed spin labeling of a genetically encoded unnatural amino acid. *Proc Natl Acad Sci U S A* **106**, 21637-21642

22. Guo, Z., Cascio, D., Hideg, K., Kalai, T., and Hubbell, W. L. (2007) Structural determinants of nitroxide motion in spin-labeled proteins: tertiary contact and solvent-inaccessible sites in helix G of T4 lysozyme. *Protein Sci* **16**, 1069-1086

23. Yu, L., Wang, W., Ling, S., Liu, S., Xiao, L., Xin, Y., Lai, C., Xiong, Y., Zhang, L., and Tian, C. (2015) CW-EPR studies revealed different motional properties and oligomeric states of

the integrin beta1a transmembrane domain in detergent micelles or liposomes. *Sci Rep* **5**, 7848

24. Kim, S. S., Upshur, M. A., Saotome, K., Sahu, I. D., McCarrick, R. M., Feix, J. B., Lorigan, G. A., and Howard, K. P. (2015) Cholesterol-Dependent Conformational Exchange of the C-Terminal Domain of the Influenza A M2 Protein. *Biochemistry* **54**, 7157-7167

25. Sahu, I. D., Craig, A. F., Dunagan, M. M., Troxel, K. R., Zhang, R., Meiberg, A. G., Harmon, C. N., McCarrick, R. M., Kroncke, B. M., Sanders, C. R., and Lorigan, G. A. (2015) Probing Structural Dynamics and Topology of the KCNE1 Membrane Protein in Lipid Bilayers via Site-Directed Spin Labeling and Electron Paramagnetic Resonance Spectroscopy. *Biochemistry* **54**, 6402-6412

26. Song, Y., Hustedt, E. J., Brandon, S., and Sanders, C. R. (2013) Competition between homodimerization and cholesterol binding to the C99 domain of the amyloid precursor protein. *Biochemistry* **52**, 5051-5064

27. Cortes, D. M., Cuello, L. G., and Perozo, E. (2001) Molecular architecture of full-length KcsA: role of cytoplasmic domains in ion permeation and activation gating. *J Gen Physiol* **117**, 165-180

28. Voss, J., He, M. M., Hubbell, W. L., and Kaback, H. R. (1996) Site-directed spin labeling demonstrates that transmembrane domain XII in the lactose permease of Escherichia coli is an alpha-helix. *Biochemistry* **35**, 12915-12918

29. L., H. W., and C., A. (1994) Investigation of structure and dynamics in membrane proteins using site-directed spin labeling. *Current Opinion in Structural Biology* **4**, 566–573

30. Hubbell, E. P. a. W. L. (1993) Transmembrane voltage control in liposomes-the use of bacteriorhodopsin as a light-driven current source. *Biophysical Journal* **64**, A222–A222

31. Sahu, I. D., Zhang, R., Dunagan, M. M., Craig, A. F., and Lorigan, G. A. (2017) Characterization of KCNE1 inside Lipodisq Nanoparticles for EPR Spectroscopic Studies of Membrane Proteins. *J Phys Chem B* **121**, 5312-5321

32. Soria, M. A., Cervantes, S. A., Bajakian, T. H., and Siemer, A. B. (2017) The Functional Amyloid Orb2A Binds to Lipid Membranes. *Biophys J* **113**, 37-47

33. McCaffrey, J. E., James, Z. M., Svensson, B., Binder, B. P., and Thomas, D. D. (2016) A bifunctional spin label reports the structural topology of phospholamban in magnetically-aligned bicelles. *J Magn Reson* **262**, 50-56

34. Sahu, I. D., Mayo, D. J., Subbaraman, N., Inbaraj, J. J., McCarrick, R. M., and Lorigan, G. A. (2017) Probing topology and dynamics of the second transmembrane domain (M2delta) of the acetyl choline receptor using magnetically aligned lipid bilayers (bicelles) and EPR spectroscopy. *Chem Phys Lipids* **206**, 9-15

35. Hustedt, E. J., and Beth, A. H. (1999) Nitroxide spin-spin interactions: applications to protein structure and dynamics. *Annu Rev Biophys Biomol Struct* **28**, 129-153

36. Hustedt, E. J., Stein, R. A., Sethaphong, L., Brandon, S., Zhou, Z., and Desensi, S. C. (2006) Dipolar coupling between nitroxide spin labels: the development and application of a tether-in-a-cone model. *Biophys J* **90**, 340-356

37. Jeschke, G. (2013) Conformational dynamics and distribution of nitroxide spin labels. *Prog Nucl Magn Reson Spectrosc* **72**, 42-60

38. DeSensi, S. C., Rangel, D. P., Beth, A. H., Lybrand, T. P., and Hustedt, E. J. (2008) Simulation of nitroxide electron paramagnetic resonance spectra from brownian trajectories and molecular dynamics simulations. *Biophys J* **94**, 3798-3809

39. Warshaviak, D. T., Serbulea, L., Houk, K. N., and Hubbell, W. L. (2011) Conformational analysis of a nitroxide side chain in an alpha-helix with density functional theory. *J Phys Chem B* **115**, 397-405

40. Tombolato, F., Ferrarini, A., and Freed, J. H. (2006) Modeling the effects of structure and dynamics of the nitroxide side chain on the ESR spectra of spin-labeled proteins. *J Phys Chem B* **110**, 26260-26271

41. Tombolato, F., Ferrarini, A., and Freed, J. H. (2006) Dynamics of the nitroxide side chain in spin-labeled proteins. *J Phys Chem B* **110**, 26248-26259

42. Sezer, D., Freed, J. H., and Roux, B. (2008) Using Markov models to simulate electron spin resonance spectra from molecular dynamics trajectories. *J Phys Chem B* **112**, 11014-11027

43. Sezer, D., Freed, J. H., and Roux, B. (2008) Parametrization, molecular dynamics simulation, and calculation of electron spin resonance spectra of a nitroxide spin label on a polyalanine alpha-helix. *J Phys Chem B* **112**, 5755-5767

44.   Islam, S. M., Stein, R. A., McHaourab, H. S., and Roux, B. (2013) Structural refinement from restrained-ensemble simulations based on EPR/DEER data: application to T4 lysozyme. *J Phys Chem B* **117**, 4740-4754

45.   Polyhach, Y., Bordignon, E., and Jeschke, G. (2011) Rotamer libraries of spin labelled cysteines for protein studies. *Phys Chem Chem Phys* **13**, 2356-2366

46.   Stoll, S., Lee, Y. T., Zhang, M., Wilson, R. F., Britt, R. D., and Goodin, D. B. (2012) Double electron-electron resonance shows cytochrome P450cam undergoes a conformational change in solution upon binding substrate. *Proc Natl Acad Sci U S A* **109**, 12888-12893

47.   Raghuraman, H., Cordero-Morales, J. F., Jogini, V., Pan, A. C., Kollewe, A., Roux, B., and Perozo, E. (2012) Mechanism of Cd2+ coordination during slow inactivation in potassium channels. *Structure* **20**, 1332-1342

48.   Cunningham, T. F., McGoff, M. S., Sengupta, I., Jaroniec, C. P., Horne, W. S., and Saxena, S. (2012) High-resolution structure of a protein spin-label in a solvent-exposed beta-sheet and comparison with DEER spectroscopy. *Biochemistry* **51**, 6350-6359

49.   Lillington, J. E., Lovett, J. E., Johnson, S., Roversi, P., Timmel, C. R., and Lea, S. M. (2011) Shigella flexneri Spa15 crystal structure verified in solution by double electron electron resonance. *J Mol Biol* **405**, 427-435

50.   Gruene, T., Cho, M. K., Karyagina, I., Kim, H. Y., Grosse, C., Giller, K., Zweckstetter, M., and Becker, S. (2011) Integrated analysis of the conformation of a protein-linked spin label by crystallography, EPR and NMR spectroscopy. *J Biomol NMR* **49**, 111-119

51.   Freed, D. M., Khan, A. K., Horanyi, P. S., and Cafiso, D. S. (2011) Molecular origin of electron paramagnetic resonance line shapes on beta-barrel membrane proteins: the local solvation environment modulates spin-label configuration. *Biochemistry* **50**, 8792-8803

52.   Kroncke, B. M., Horanyi, P. S., and Columbus, L. (2010) Structural origins of nitroxide side chain dynamics on membrane protein alpha-helical sites. *Biochemistry* **49**, 10045-10060

53.   Freed, D. M., Horanyi, P. S., Wiener, M. C., and Cafiso, D. S. (2010) Conformational exchange in a membrane transport protein is altered in protein crystals. *Biophys J* **99**, 1604-1610

54.   Fleissner, M. R., Cascio, D., and Hubbell, W. L. (2009) Structural origin of weakly ordered nitroxide motion in spin-labeled proteins. *Protein Sci* **18**, 893-908

55. Guo, Z., Cascio, D., Hideg, K., and Hubbell, W. L. (2008) Structural determinants of nitroxide motion in spin-labeled proteins: solvent-exposed sites in helix B of T4 lysozyme. *Protein Sci* **17**, 228-239

56. Langen, R., Oh, K. J., Cascio, D., and Hubbell, W. L. (2000) Crystal structures of spin labeled T4 lysozyme mutants: implications for the interpretation of EPR spectra in terms of structure. *Biochemistry* **39**, 8396-8405

57. Beier, C., and Steinhoff, H. J. (2006) A structure-based simulation approach for electron paramagnetic resonance spectra using molecular and stochastic dynamics simulations. *Biophys J* **91**, 2647-2664

58. Sezer, D., Freed, J. H., and Roux, B. (2009) Multifrequency electron spin resonance spectra of a spin-labeled protein calculated from molecular dynamics simulations. *J Am Chem Soc* **131**, 2597-2605

59. Jo, S., Kim, T., Iyer, V. G., and Im, W. (2008) CHARMM-GUI: a web-based graphical user interface for CHARMM. *J Comput Chem* **29**, 1859-1865

60. William L. Jorgensen , J. C., Jeffry D. Madura , Roger W. Impey , Michael L. Klein. (1983) Comparison of simple potential functions for simulating liquid water. *The Journal of Chemical Physics* **79**, 926-935

61. Phillips, J. C., Braun, R., Wang, W., Gumbart, J., Tajkhorshid, E., Villa, E., Chipot, C., Skeel, R. D., Kale, L., and Schulten, K. (2005) Scalable molecular dynamics with NAMD. *J Comput Chem* **26**, 1781-1802

62. Klauda, J. B., Venable, R. M., Freites, J. A., O'Connor, J. W., Tobias, D. J., Mondragon-Ramirez, C., Vorobyov, I., MacKerell, A. D., Jr., and Pastor, R. W. (2010) Update of the CHARMM all-atom additive force field for lipids: validation on six lipid types. *J Phys Chem B* **114**, 7830-7843

63. Ulrich Essmann, L. P., and Max L. Berkowitz. (1995) A smooth particle mesh Ewald method. *J. Chem. Phys.* **103**, 8577–8593

64. van Gunsteren, W. F. B., H. J. C. (1977) Algorithms for macromolecular dynamics and constraint dynamics. *Molecular Physics* **34**, 1311-1327

65.   Robert R. Fraser, G. B., John K. Saunders, Joseph B. Lambert, and Craig E. Mixan. (1971) Barriers to rotation about the sulfur-sulfur bond in acyclic disulfides. *Journal of the American Chemical Society* **93**, 3822-3823

จุฬาลงกรณ์มหาวิทยาลัย
CHULALONGKORN UNIVERSITY

VITA

NAME	Ngoc Lan Le Nguyen
DATE OF BIRTH	20 October 1995
PLACE OF BIRTH	Phu Cat district, Binh Dinh province, Vietnam
INSTITUTIONS ATTENDED	Department of Chemistry, Faculty of Science, Chulalongkorn University
HOME ADDRESS	488/18 Phetchaburi Road, Thung Phaya Thai, Khet Ratchathewi, Bangkok 10400

จุฬาลงกรณ์มหาวิทยาลัย
CHULALONGKORN UNIVERSITY